Available online at www.sciencedirect.com
ScienceDirect
Nonlinear Analysis: Real World Applications 8 (2007) 1431 – 1458
Nonlinear Analysis
Real World Applications
www.elsevier.com/locate/na

Fluid-structure interaction with applications in biomechanics

Jaroslav Hron[a,*], Martin Mádlík[b]

[a] *Institute of Applied Mathematics, University of Dortmund, Vogelpothsweg 87, 44227 Dortmund, Germany*
[b] *Mathematical Institute, Charles University, Sokolovská 83, 186 75 Prague, Czech Republic*

Received 22 May 2006; accepted 30 May 2006

Abstract

In bioengineering applications problems of flow interacting with elastic solid are very common. We formulate the problem of interaction for an incompressible fluid and an incompressible elastic material in a fully coupled arbitrary Lagrangian–Eulerian (ALE) formulation. The mathematical description and the numerical schemes are designed in such a way that more complicated constitutive relations (and more realistic for bioengineering applications) can be incorporated easily. The whole domain of interest is treated as one continuum and the same discretization in space (FEM) and time (Crank–Nicholson) is used for both, solid and fluid, parts. The resulting nonlinear algebraic system is solved by an approximate Newton method. The combination of second order discretization and fully coupled solution method gives a method with high accuracy and robustness. To demonstrate the flexibility of this numerical approach we apply the same method to a mixture-based model of an elastic material with perfusion which also falls into the category of fluid structure interactions. A few simple example calculations with simple material models and large deformations of the solid part are presented.

Keywords: Fluid-structure interaction; Monolithic ALE method; Biomechanics

1. Overview

Both problems of viscous fluid flow and of elastic body deformation have been studied separately for many years in great detail. But there are many problems encountered in real life where an interaction between those two media is of great importance. A typical example of such a problem is the area of aero-elasticity. Another important area where such interaction is of great interest is biomechanics. Such interaction is encountered especially when dealing with the blood circulatory system. Problems of a pulsatile flow in an elastic tube, flow through heart valves, flow in the heart chambers are some of the examples. In all these cases we have to deal with large deformations of a deformable solid interacting with an unsteady, often periodic, fluid flow. The ability to model and predict the mechanical behavior of biological tissues is very important in several areas of bio-engineering and medicine. For example, a good mathematical model for biological tissue could be used in such areas as early recognition or prediction of heart muscle failure, advanced design of new treatments and operative procedures, and the understanding of atherosclerosis and associated problems. Other possible applications include development of virtual reality programs for training new surgeons or designing new operative procedures (see [23,25]), and last but not least the design of medical instruments or artificial replacements

* Corresponding author.
E-mail address: hron@math.uni-dortmund.de (J. Hron).

1468-1218/$ - see front matter © 2006 Elsevier Ltd. All rights reserved.
doi:10.1016/j.nonrwa.2006.05.007

with optimal mechanical and other properties as close as possible to the original parts (see [45]). These are some of the areas where a good mathematical model of soft tissue with reliable and fast numerical solution is essential for success.

A numerical solution of the resulting equations of the fluid structure interaction problem poses a great challenge since it includes the features of nonlinear elasticity, fluid mechanics and their coupling. The easiest solution strategy, mostly used in the available software packages, is to decouple the problem into the fluid part and solid part, for each of those parts to use some well established method of solution then the interaction is introduced as external boundary conditions in each of the subproblems. This has an advantage that there are many well tested finite element based numerical methods for separate problems of fluid flow and elastic deformation, on the other hand the treatment of the interface and the interaction is problematic especially in the case when the characteristics of the two interacting materials are similar which is the case in many biomechanical applications. The approach presented here treats the problem as a single continuum with the coupling automatically taken care of as internal interface, which in our formulation does not require any special treatment.

1.1. Fluid structure models

There have been several different approaches to the problem of fluid-structure interaction. Most notably these include the work of [27–30] where an immersed boundary method was developed and applied to a three-dimensional model of the heart. In this model they consider a set of one-dimensional elastic fibers immersed in three-dimensional fluid region and using a parallel supercomputer they were able to model the pulse of the heart ventricle. Their method can capture the anisotropy caused by the muscle fibers.

A fluid-structure model with the wall modeled as a thin shell was used to model the left heart ventricle in [5,6] and [32,31]. In [13,14] similar approach was used to model a flow in a collapsible tubes. In these models the wall is modeled by two-dimensional thin shell which can be modified to capture the anisotropy of the muscle. In reality the thickness of the wall can be significant and very important. For example in arteries the wall thickness can be up to 30% of the diameter and its local thickening can be the cause of an aneurysm creation. In the case of heart ventricle the thickness of the wall is also significant and also the direction of the muscle fibers changes through the wall.

Actual three-dimensional approximation is up to now very rare. The most common approach is the combination of separate solvers for fluid and solid by an outer coupling iteration (see [26] for more details).

1.2. Mixture models for perfusion

Another class of models which fall into the fluid structure interaction problems are the fluid–solid mixture models used for simulation of soft tissue perfusion like muscles or cartilage. Mixture theory was first applied to swelling and diffusion in rubber materials [7,33], mechanics of skin [24], compression of cartilage [39,19,34] and blood perfusion through biological tissues in [42,43]. (see for example [10,22]) The basic idea of mixture theory is the assumption of co-occupancy, i.e., at each spatial point there is certain fraction of each constituent (with associated fields) and there are prescribed balance equations for each constituent of the mixture as is usual for a single continuum, with additional terms representing the interaction between constituents within the mixture.

There have been several numerical studies of mixture models. One-dimensional diffusion of fluid through an isotropic material is solved in [37], for transversely isotropic materials in [7,34] a one-dimensional diffusion through isotropic stretched slab is solved using a velocity boundary condition. Finite element solutions of mixture models for the small deformation, linear elastic case are presented in [19,43] and for nonlinear large deformation description of various soft tissues in [39,38,40,8,44,1,21].

1.3. Theoretical results

The theoretical investigation of the fluid structure interaction problems is complicated by the need of mixed description. While for the solid part the natural view is the material (Lagrangian) description for the fluid it is the spatial (Eulerian) description. In the case of their combination some kind of mixed description (usually referred to as the arbitrary Lagrangian–Eulerian (ALE) description) has to be used which brings additional nonlinearity into the resulting equations. In [20] a time dependent, linearized model of interaction between a viscous fluid and an elastic shell in small displacement approximation and its discretization is analyzed. The problem is further simplified by neglecting

all changes in the geometry configuration. Under these simplifications by using energy estimates they are able to show that the proposed formulation is well posed and a global weak solution exists. Further they show that an independent discretization by standard mixed finite elements for the fluid and by nonconforming discrete Kirchhoff triangle finite elements for the shell together with backward or central difference approximation of the time derivatives converges to the solution of the continuous problem. In [35] a steady problem of equilibrium of an elastic fixed obstacle surrounded by a viscous fluid is studied. Existence of an equilibrium state is shown with the displacement and velocity in $C^{2,\alpha}$ and pressure in $C^{1,\alpha}$ under assumption of small data in $C^{2,\alpha}$ and the domain boundaries of class C^3.

In the following section we will summarize the basic notation and setup used in this work for continuum description. Then the monolithic formulation of the continuous problem and its discretization is introduced in Section 3. To illustrate the flexibility of our discretization and solution approach we apply the same methods to the perfusion problem in Section 4. The last section shows several prototypical configurations solved by the presented method.

2. Continuum description

Let $\Omega \subset \mathbb{R}^3$ be a reference configuration of a given body, possibly an abstract one. Let $\Omega_t \subset \mathbb{R}^3$ be a configuration of this body at time t. Then a one-to-one, sufficiently smooth mapping $\vec{\chi}_\Omega$ of the reference configuration Ω to the current configuration

$$\vec{\chi}_\Omega : \Omega \times [0, T] \mapsto \Omega_t, \tag{1}$$

describes the motion of the body, see Fig. 1. The mapping $\vec{\chi}_\Omega$ depends on the choice of the reference configuration Ω which can be fixed in a various ways. Here we think of Ω to be the initial (stress-free) configuration Ω_0. Thus, if not emphasized, we mean by $\vec{\chi}$ exactly $\vec{\chi}_\Omega = \vec{\chi}_{\Omega_0}$.

If we denote by $\vec{X}$ a material point in the reference configuration Ω then the position of this point at time t is given by

$$\vec{x} = \vec{\chi}(\vec{X}, t). \tag{2}$$

Next, the mechanical fields describing the deformation are defined in a standard manner. The displacement field, the velocity field, deformation gradient and its determinant are

$$\vec{u}(\vec{X}, t) = \vec{\chi}(\vec{X}, t) - \vec{X}, \quad \vec{v} = \frac{\partial \vec{\chi}}{\partial t}, \quad \boldsymbol{F} = \frac{\partial \vec{\chi}}{\partial \vec{X}}, \quad J = \det \boldsymbol{F}. \tag{3}$$

Let us adopt following useful notations for some derivatives. Any field quantity φ with values in some vector space Y (i.e. scalar, vector or tensor valued) can be expressed in the Eulerian description as a function of the spatial position $\vec{x} \in \mathbb{R}^3$

$$\varphi = \tilde{\varphi}(\vec{x}, t) : \Omega_t \times [0, T] \mapsto Y.$$

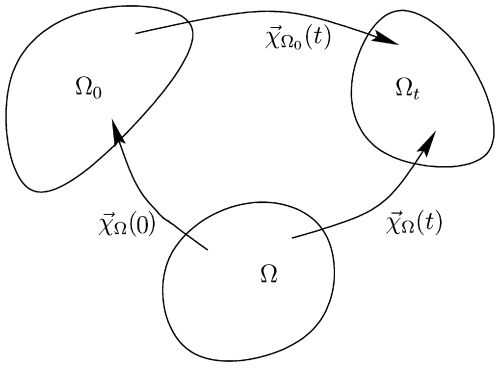

Fig. 1. The referential domain Ω, initial Ω_0 and current state Ω_t and relations between them. The identification $\Omega \equiv \Omega_0$ is adopted in this text.

Then we define following notations for the derivatives of the field φ

$$\frac{\partial \varphi}{\partial t} := \frac{\partial \tilde{\varphi}}{\partial t}, \quad \nabla \varphi = \frac{\partial \varphi}{\partial \vec{x}} := \frac{\partial \tilde{\varphi}}{\partial \vec{x}}, \quad \operatorname{div} \varphi := \operatorname{tr} \nabla \varphi. \tag{4}$$

In the case of Lagrangian description we consider the quantity φ to be defined on the reference configuration Ω, then for any $\vec{X} \in \Omega$ we can express the quantity φ as

$$\varphi = \bar{\varphi}(\vec{X}, t) : \Omega \times [0, T] \mapsto Y$$

and we define the derivatives of the field φ as

$$\frac{\mathrm{d}\varphi}{\mathrm{d}t} := \frac{\partial \bar{\varphi}}{\partial t}, \quad \operatorname{Grad} \varphi = \frac{\partial \varphi}{\partial \vec{X}} := \frac{\partial \bar{\varphi}}{\partial \vec{X}}, \quad \operatorname{Div} \varphi := \operatorname{tr} \operatorname{Grad} \varphi. \tag{5}$$

These two descriptions can be related to each other through following relations

$$\bar{\varphi}(\vec{X}, t) = \tilde{\varphi}(\vec{\chi}(\vec{X}, t), t), \tag{6}$$

$$\frac{\mathrm{d}\varphi}{\mathrm{d}t} = \frac{\partial \varphi}{\partial t} + (\nabla \varphi)\vec{v}, \quad \operatorname{Grad} \varphi = (\nabla \varphi)\boldsymbol{F}, \quad \int_{\Omega_t} \varphi \, \mathrm{d}v = \int_{\Omega} \varphi J \, \mathrm{d}V, \tag{7}$$

$$\frac{\mathrm{d}\boldsymbol{F}}{\mathrm{d}t} = \operatorname{Grad} \vec{v}, \quad \frac{\partial J}{\partial \boldsymbol{F}} = J\boldsymbol{F}^{-T}, \quad \frac{\mathrm{d}J}{\mathrm{d}t} = J \operatorname{div} \vec{v}. \tag{8}$$

For the formulation of the balance laws we will need to express a time derivatives of some integrals. The following series of equalities obtained by using the previously stated relations will be useful

$$\begin{aligned} \frac{\mathrm{d}}{\mathrm{d}t} \int_{\Omega_t} \varphi \, \mathrm{d}v &= \frac{\mathrm{d}}{\mathrm{d}t} \int_{\Omega} \varphi J \, \mathrm{d}V = \int_{\Omega} \frac{\mathrm{d}}{\mathrm{d}t}(\varphi J) \, \mathrm{d}V = \int_{\Omega_t} \left(\frac{\mathrm{d}\varphi}{\mathrm{d}t} + \varphi \operatorname{div} \vec{v} \right) \mathrm{d}v \\ &= \int_{\Omega_t} \left(\frac{\partial \varphi}{\partial t} + \operatorname{div}(\varphi \vec{v}) \right) \mathrm{d}v = \int_{\Omega_t} \frac{\partial \varphi}{\partial t} \, \mathrm{d}v + \int_{\partial \Omega_t} \varphi \vec{v} \cdot \vec{n} \, \mathrm{d}a \\ &= \frac{\partial}{\partial t} \int_{\Omega_t} \varphi \, \mathrm{d}v + \int_{\partial \Omega_t} \varphi \vec{v} \cdot \vec{n} \, \mathrm{d}a. \end{aligned} \tag{9}$$

And also the Piola identity will be used $\operatorname{Div}(J\boldsymbol{F}^{-T}) = \vec{0}$, which can be checked by differentiating the left-hand side and using (8) together with an identity obtained by differentiating the relation $\boldsymbol{F}\boldsymbol{F}^{-1} = \boldsymbol{I}$.

2.1. Balance laws

In this section we will formulate the balance relations for mass and momentum in three forms: the Eulerian, the Lagrangian and the ALE description.

The Eulerian (or spatial) description is well suited for a problem of fluid flowing through some spatially fixed region. In such a case the material particles can enter and leave the region of interest. The fundamental quantity describing the motion is the velocity vector.

On the other hand the Lagrangian (or referential) description is well suited for a problem of deforming a given body consisting of a fixed set of material particles. In this case the actual boundary of the body can change its shape. The fundamental quantity describing the motion in this case is the vector of displacement from the referential state.

In the case of fluid-structure interaction problem we can still use the Lagrangian description for the deformation of the solid part. The fluid flow now takes place in a domain with boundary given by the deformation of the structure which can change in time and is influenced back by the fluid flow. The mixed ALE description of the fluid has to be used in this case. The fundamental quantity describing the motion of the fluid is still the velocity vector but the description is accompanied by a certain displacement field which describes the change of the fluid domain. This displacement field has no connection to the fluid velocity field and the purpose of its introduction is to provide a transformation

of the current fluid domain and corresponding governing equations to some fixed reference domain. This method is sometimes called a pseudo-solid mapping method (see [36]).

Let $\mathscr{P} \subset \mathbb{R}^3$ be a fixed region in space (a control volume) with the boundary $\partial\mathscr{P}$ and unit outward normal vector $\vec{n}_{\mathscr{P}}$, such that

$$\mathscr{P} \subset \Omega_t \quad \text{for all } t \in [0, T].$$

Let ϱ denote the mass density of the material. Then the balance of mass in the region $\mathscr{P}$ can be written as

$$\frac{\partial}{\partial t}\int_{\mathscr{P}} \varrho \,\mathrm{d}v + \int_{\partial\mathscr{P}} \varrho\vec{v}\cdot\vec{n}_{\mathscr{P}}\,\mathrm{d}a = 0. \tag{10}$$

If all the fields are sufficiently smooth this equation can be written in local form with respect to the current configuration as

$$\frac{\partial\varrho}{\partial t} + \operatorname{div}(\varrho\vec{v}) = 0. \tag{11}$$

It will be useful to derive the mass balance equation from the Lagrangian point of view. Let $\mathscr{Q} \subset \Omega$ be a fixed set of particles. Then $\vec{\chi}(\mathscr{Q}, t) \subset \Omega_t$ is a region occupied by these particles at the time t, and the balance of mass can be expressed as

$$\frac{\mathrm{d}}{\mathrm{d}t}\int_{\vec{\chi}(\mathscr{Q},t)} \varrho \,\mathrm{d}v = 0, \tag{12}$$

which in local form with respect to the reference configuration can be written as

$$\frac{\mathrm{d}}{\mathrm{d}t}(\varrho J) = 0. \tag{13}$$

In the case of an ALE description we take a region $\mathscr{Z} \subset \mathbb{R}^3$ which is itself moving independently of the motion of the body. Let the motion of the control region $\mathscr{Z}$ be described by a given mapping

$$\vec{\zeta}_{\mathscr{Z}} : \mathscr{Z} \times [0, T] \mapsto \mathscr{Z}_t, \quad \mathscr{Z}_t \subset \Omega_t \ \ \forall t \in [0, T],$$

with the corresponding velocity $\vec{v}_{\mathscr{Z}} = \partial\vec{\zeta}_{\mathscr{Z}}/\partial t$, deformation gradient $\boldsymbol{F}_{\mathscr{Z}} = \partial\vec{\zeta}_{\mathscr{Z}}/\partial\vec{X}$ and its determinant $J_{\mathscr{Z}} = \det \boldsymbol{F}_{\mathscr{Z}}$. The mass balance equation can be written as

$$\frac{\partial}{\partial t}\int_{\mathscr{Z}_t} \varrho \,\mathrm{d}v + \int_{\partial\mathscr{Z}_t} \varrho(\vec{v} - \vec{v}_{\mathscr{Z}})\cdot\vec{n}_{\mathscr{Z}_t}\,\mathrm{d}a = 0 \tag{14}$$

this can be viewed as an Eulerian description with a moving spatial coordinate system or as a grid deformation in the context of the finite element method. In order to obtain a local form of the balance relation we need to transform the integration to the fixed spatial region $\mathscr{Z}$

$$\frac{\partial}{\partial t}\int_{\mathscr{Z}} \varrho J_{\mathscr{Z}} \,\mathrm{d}v + \int_{\partial\mathscr{Z}} \varrho(\vec{v} - \vec{v}_{\mathscr{Z}})\cdot\boldsymbol{F}_{\mathscr{Z}}^{-T}\vec{n}_{\mathscr{Z}} J_{\mathscr{Z}}\,\mathrm{d}a = 0, \tag{15}$$

then the local form is

$$\frac{\partial}{\partial t}(\varrho J_{\mathscr{Z}}) + \operatorname{div}(\varrho J_{\mathscr{Z}}(\vec{v} - \vec{v}_{\mathscr{Z}})\boldsymbol{F}_{\mathscr{Z}}^{-T}) = 0. \tag{16}$$

The two previous special formulations can be now recovered. If the region $\mathscr{Z}$ is not moving in space, i.e. $\mathscr{Z} = \mathscr{Z}_t, \forall t \in [0, T]$, then $\vec{\zeta}_{\mathscr{Z}}$ is the identity mapping, $\boldsymbol{F}_{\mathscr{Z}} = \boldsymbol{I}$, $J_{\mathscr{Z}} = 1$, $\vec{v}_{\mathscr{Z}} = \vec{0}$ and (16) reduces to (11). While, if the region $\mathscr{Z}$ moves exactly with the material, i.e. $\vec{\zeta}_{\mathscr{Z}} = \vec{\chi}|_{\mathscr{Z}}$ then $\boldsymbol{F}_{\mathscr{Z}} = \boldsymbol{F}$, $J_{\mathscr{Z}} = J$, $\vec{v}_{\mathscr{Z}} = \vec{v}$ and (16) reduces to (13).

The balance of linear momentum is postulated in a similar way. Let $\boldsymbol{\sigma}$ denote the Cauchy stress tensor field, representing the surface forces per unit area, $\vec{f}$ be the body forces acting on the material per unit mass. Then the balance of linear momentum in the Eulerian description is stated as

$$\frac{\partial}{\partial t}\int_{\mathscr{P}} \varrho\vec{v}\,\mathrm{d}v + \int_{\partial\mathscr{P}} \varrho\vec{v}\otimes\vec{v}\vec{n}_{\mathscr{P}}\,\mathrm{d}a = \int_{\partial\mathscr{P}} \boldsymbol{\sigma}^T\vec{n}_{\mathscr{P}}\,\mathrm{d}a + \int_{\mathscr{P}} \varrho\vec{f}\,\mathrm{d}v. \tag{17}$$

The local form of the linear momentum balance is

$$\frac{\partial\varrho\vec{v}}{\partial t} + \operatorname{div}(\varrho\vec{v}\otimes\vec{v}) = \operatorname{div}\boldsymbol{\sigma}^T + \varrho\vec{f} \tag{18}$$

or with the use of (11) we can write

$$\varrho\frac{\partial\vec{v}}{\partial t} + \varrho(\nabla\vec{v})\vec{v} = \operatorname{div}\boldsymbol{\sigma}^T + \varrho\vec{f}. \tag{19}$$

From the Lagrangian point of view the momentum balance relation is

$$\frac{\mathrm{d}}{\mathrm{d}t}\int_{\vec{\chi}(Q,t)} \varrho\vec{v}\,\mathrm{d}v = \int_{\partial\vec{\chi}(Q,t)} \boldsymbol{\sigma}^T\vec{n}_{\vec{\chi}(Q,t)}\,\mathrm{d}a + \int_{\vec{\chi}(Q,t)} \varrho\vec{f}\,\mathrm{d}v. \tag{20}$$

Let us denote by $\boldsymbol{P} = J\boldsymbol{\sigma}^T\boldsymbol{F}^{-T}$ the first Piola–Kirchhoff stress tensor (see [12]), then the local form of the momentum balance is

$$\frac{\mathrm{d}}{\mathrm{d}t}(\varrho J\vec{v}) = \operatorname{Div}\boldsymbol{P} + \varrho J\vec{f} \tag{21}$$

or using (13) we can write

$$\varrho J\,\frac{\mathrm{d}\vec{v}}{\mathrm{d}t} = \operatorname{Div}\boldsymbol{P} + \varrho J\vec{f}. \tag{22}$$

In the ALE formulation we obtain

$$\frac{\partial}{\partial t}\int_{\mathscr{X}_t} \varrho\vec{v}\,\mathrm{d}v + \int_{\partial\mathscr{X}_t} \varrho\vec{v}\otimes(\vec{v}-\vec{v}_{\mathscr{X}})\vec{n}_{\mathscr{X}_t}\mathrm{d}a = \int_{\partial\mathscr{X}_t} \boldsymbol{\sigma}^T\vec{n}_{\mathscr{X}_t}\mathrm{d}a + \int_{\mathscr{X}_t} \varrho\vec{f}\,\mathrm{d}v \tag{23}$$

which in the local form gives

$$\frac{\partial\varrho J_{\mathscr{X}}\vec{v}}{\partial t} + \operatorname{div}\left(\varrho J_{\mathscr{X}}\vec{v}\otimes(\vec{v}-\vec{v}_{\mathscr{X}})\boldsymbol{F}_{\mathscr{X}}^{-T}\right) = \operatorname{div}\left(J_{\mathscr{X}}\boldsymbol{\sigma}^T\boldsymbol{F}_{\mathscr{X}}^{-T}\right) + \varrho J_{\mathscr{X}}\vec{f} \tag{24}$$

or with the use of (16) we can write

$$\varrho J_{\mathscr{X}}\frac{\partial\vec{v}}{\partial t} + \varrho J_{\mathscr{X}}\,(\nabla\vec{v})\,\boldsymbol{F}_{\mathscr{X}}^{-T}\left(\vec{v}-\vec{v}_{\mathscr{X}}\right) = \operatorname{div}\left(J_{\mathscr{X}}\boldsymbol{\sigma}^T\boldsymbol{F}_{\mathscr{X}}^{-T}\right) + \varrho J_{\mathscr{X}}\vec{f}. \tag{25}$$

In the case of angular momentum balance we assume that there are no external or internal sources of angular momentum. It then follows that the Cauchy stress tensor has to be symmetric, i.e. $\boldsymbol{\sigma} = \boldsymbol{\sigma}^T$. Assuming isothermal conditions the energy balance is satisfied and the choice of the constitutive relations for the materials has to be compatible with the balance of entropy (see [41]).

3. Fluid structure interaction problem formulation

At this point we make a few assumptions that will allow us to deal with the task of setting up a tractable problem. Let us consider a flow between thick elastic walls as shown in Fig. 2. We will use the superscripts $^{\mathrm{s}}$ and $^{\mathrm{f}}$ to denote the quantities connected with the solid and fluid. Let us assume that both materials are incompressible and all the processes are isothermal, which is a well accepted approximation in biomechanics, and let us denote the constant densities of each material by ϱ^{f}, ϱ^{s}.

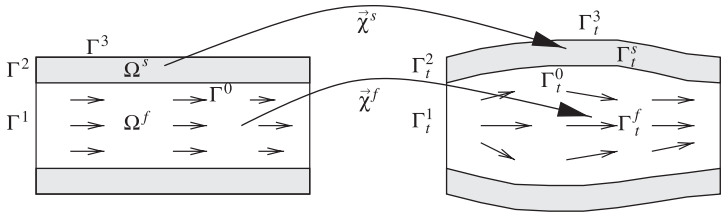

Fig. 2. Undeformed (original) and deformed (current) configurations.

3.1. Monolithic description

We denote by Ω_t^{f} the domain occupied by the fluid and Ω_t^{s} by the solid at time $t \in [0, T]$. Let $\Gamma_t^0 = \bar{\Omega}_t^{\mathrm{f}} \cap \bar{\Omega}_t^{\mathrm{s}}$ be the part of the boundary where the solid interacts with the fluid and Γ_t^i, $i = 1, 2, 3$ be the remaining external boundaries of the solid and the fluid as depicted in Fig. 2.

Let the deformation of the solid part be described by the mapping $\vec{\chi}^{\mathrm{s}}$

$$\vec{\chi}^{\mathrm{s}} : \Omega^{\mathrm{s}} \times [0, T] \mapsto \Omega_t^{\mathrm{s}}, \tag{26}$$

with the corresponding displacement $\vec{u}^{\mathrm{s}}$ and the velocity $\vec{v}^{\mathrm{s}}$ given by

$$\vec{u}^{\mathrm{s}}(\vec{X}, t) = \vec{\chi}^{\mathrm{s}}(\vec{X}, t) - \vec{X}, \quad \vec{v}^{\mathrm{s}}(\vec{X}, t) = \frac{\partial \vec{\chi}^{\mathrm{s}}}{\partial t}(\vec{X}, t). \tag{27}$$

The fluid flow is described by the velocity field $\vec{v}^{\mathrm{f}}$ defined on the fluid domain Ω_t^{f}

$$\vec{v}^{\mathrm{f}}(\vec{x}, t) : \Omega_t^{\mathrm{f}} \times [0, T] \mapsto \mathbb{R}^3. \tag{28}$$

Further we define the auxiliary mapping, denoted by $\vec{\zeta}^{\mathrm{f}}$, to describe the change of the fluid domain and corresponding displacement $\vec{u}^{\mathrm{f}}$ by

$$\vec{\zeta}^{\mathrm{f}} : \Omega^{\mathrm{f}} \times [0, T] \mapsto \Omega_t^{\mathrm{f}}, \quad \vec{u}^{\mathrm{f}}(\vec{X}, t) = \vec{\zeta}^{\mathrm{f}}(\vec{X}, t) - \vec{X}. \tag{29}$$

We require that the mapping $\vec{\zeta}^{\mathrm{f}}$ is sufficiently smooth, one to one and has to satisfy

$$\vec{\zeta}^{\mathrm{f}}(\vec{X}, t) = \vec{\chi}^{\mathrm{s}}(\vec{X}, t), \quad \forall (\vec{X}, t) \in \Gamma^0 \times [0, T]. \tag{30}$$

In the context of the finite element method this will describe the artificial mesh deformation inside the fluid region and it will be constructed as a solution to a suitable boundary value problem with (30) as the boundary condition.

The momentum and mass balance of the fluid in the time dependent fluid domain according to (16) and (24) are

$$\varrho^{\mathrm{f}} \frac{\partial \vec{v}^{\mathrm{f}}}{\partial t} + \varrho^{\mathrm{f}} (\nabla \vec{v}^{\mathrm{f}}) \left(\vec{v}^{\mathrm{f}} - \frac{\partial \vec{u}^{\mathrm{f}}}{\partial t} \right) = \operatorname{div} \boldsymbol{\sigma}^{\mathrm{f}} \quad \text{in } \Omega_t^{\mathrm{f}}, \tag{31}$$

$$\operatorname{div} \vec{v}^{\mathrm{f}} = 0 \quad \text{in } \Omega_t^{\mathrm{f}}, \tag{32}$$

together with the momentum (18) and mass (11) balance of the solid in the solid domain

$$\varrho^{\mathrm{s}} \frac{\partial \vec{v}^{\mathrm{s}}}{\partial t} + \varrho^{\mathrm{s}} (\nabla \vec{v}^{\mathrm{s}}) \vec{v}^{\mathrm{s}} = \operatorname{div} \boldsymbol{\sigma}^{\mathrm{s}} \quad \text{in } \Omega_t^{\mathrm{s}}, \tag{33}$$

$$\operatorname{div} \vec{v}^{\mathrm{s}} = 0 \quad \text{in } \Omega_t^{\mathrm{s}}. \tag{34}$$

The interaction is due to the exchange of momentum through the common part of the boundary Γ_t^0. On this part we require that the forces are in balance and simultaneously the no slip boundary condition holds for the fluid, i.e.

$$\boldsymbol{\sigma}^{\mathrm{f}} \vec{n} = \boldsymbol{\sigma}^{\mathrm{s}} \vec{n} \quad \text{on } \Gamma_t^0, \quad \vec{v}^{\mathrm{f}} = \vec{v}^{\mathrm{s}} \quad \text{on } \Gamma_t^0. \tag{35}$$

The remaining external boundary conditions can be of the following kind. A natural boundary condition on the fluid inflow and outflow part Γ_t^1

$$\boldsymbol{\sigma}^{\mathrm{f}}\vec{n} = p_{\mathrm{B}}\vec{n} \quad \text{on } \Gamma_t^1 \tag{36}$$

with p_{B} given value. Alternatively we can prescribe a Dirichlet type boundary condition on the inflow or outflow part Γ_t^1

$$\vec{v}^{\mathrm{f}} = \vec{v}_{\mathrm{B}} \quad \text{on } \Gamma_t^1, \tag{37}$$

where $\vec{v}_{\mathrm{B}}$ is given. The Dirichlet boundary condition is prescribed for the solid displacement at the part Γ_t^2

$$\vec{u}^{\mathrm{s}} = \vec{0} \quad \text{on } \Gamma_t^2 \tag{38}$$

and the stress free boundary condition for the solid is applied at the part Γ_t^3

$$\boldsymbol{\sigma}^{\mathrm{s}}\vec{n} = \vec{0} \quad \text{on } \Gamma_t^3. \tag{39}$$

We introduce the domain $\Omega = \Omega^{\mathrm{f}} \cup \Omega^{\mathrm{s}}$, where $\Omega^{\mathrm{f}}, \Omega^{\mathrm{s}}$ are the domains occupied by the fluid and solid in the initial undeformed state, and two fields defined on this domain as

$$\vec{u} : \Omega \times [0, T] \to \mathbb{R}^3, \quad \vec{v} : \Omega \times [0, T] \to \mathbb{R}^3$$

such that the field $\vec{v}$ represents the velocity at the given point and $\vec{u}$ the displacement on the solid part and the artificial displacement in the fluid part, taking care of the fact that the fluid domain is changing with time,

$$\vec{v} = \begin{cases} \vec{v}^{\mathrm{s}} & \text{on } \Omega^{\mathrm{s}}, \\ \vec{v}^{\mathrm{f}} & \text{on } \Omega^{\mathrm{f}}, \end{cases} \quad \vec{u} = \begin{cases} \vec{u}^{\mathrm{s}} & \text{on } \Omega^{\mathrm{s}}, \\ \vec{u}^{\mathrm{f}} & \text{on } \Omega^{\mathrm{f}}. \end{cases} \tag{40}$$

Due to the conditions (30) and (35) both fields are continuous across the interface Γ_t^0 and we can define global quantities on Ω as the deformation gradient and its determinant

$$\boldsymbol{F} = \boldsymbol{I} + \operatorname{Grad}\vec{u}, \quad J = \det \boldsymbol{F}. \tag{41}$$

Using this notation the solid balance laws (33) and (34) can be expressed in the Lagrangian formulation with the initial configuration Ω^{s} as reference, cf. (21),

$$J\varrho^{\mathrm{s}}\frac{\mathrm{d}\vec{v}}{\mathrm{d}t} = \operatorname{Div}\boldsymbol{P}^{\mathrm{s}} \quad \text{in } \Omega^{\mathrm{s}}, \tag{42}$$

$$J = 1 \quad \text{in } \Omega^{\mathrm{s}}. \tag{43}$$

The fluid equations (31) and (32) are already expressed in the ALE formulation with respect to the time dependent region Ω_t^{f}, now we transform the equations to the fixed initial region Ω^{f} by the mapping ζ^{f} defined by (29)

$$\varrho^{\mathrm{f}}\frac{\partial\vec{v}}{\partial t} + \varrho^{\mathrm{f}}(\operatorname{Grad}\vec{v})\boldsymbol{F}^{-1}\left(\vec{v} - \frac{\partial\vec{u}}{\partial t}\right) = J^{-1}\operatorname{Div}(J\boldsymbol{\sigma}^{\mathrm{f}}F^{-T}) \quad \text{in } \Omega^{\mathrm{f}}, \tag{44}$$

$$\operatorname{Div}(J\vec{v}\boldsymbol{F}^{-T}) = 0 \quad \text{in } \Omega^{\mathrm{f}}. \tag{45}$$

It remains to prescribe some relation for the mapping ζ^{f}. In terms of the corresponding displacement $\vec{u}^{\mathrm{f}}$ we formulate some simple relation together with the Dirichlet boundary conditions required by (30), for example

$$\frac{\partial\vec{u}}{\partial t} = \Delta\vec{u} \text{ in } \Omega^{\mathrm{f}}, \quad \vec{u} = \vec{u}^{\mathrm{s}} \text{ on } \Gamma^0, \quad \vec{u} = \vec{0} \text{ on } \Gamma^1. \tag{46}$$

Other choices are possible. For example, the mapping $\vec{u}^{\mathrm{f}}$ can be realized as a solution of the elasticity problem with the same Dirichlet boundary conditions. (see [36]).

The complete set of the equations can be written as

$$\frac{\partial \vec{u}}{\partial t} = \begin{cases} \vec{v} & \text{in } \Omega^{\mathrm{s}}, \\ \Delta \vec{u} & \text{in } \Omega^{\mathrm{f}}, \end{cases} \tag{47}$$

$$\frac{\partial \vec{v}}{\partial t} = \begin{cases} \dfrac{1}{J\varrho^{\mathrm{s}}} \operatorname{Div} \boldsymbol{P}^{\mathrm{s}} & \text{in } \Omega^{\mathrm{s}}, \\ -(\operatorname{Grad} \vec{v})\boldsymbol{F}^{-1}\left(\vec{v} - \dfrac{\partial \vec{u}}{\partial t}\right) + \dfrac{1}{J\varrho^{\mathrm{f}}} \operatorname{Div}(J\boldsymbol{\sigma}^{\mathrm{f}}\boldsymbol{F}^{-T}) & \text{in } \Omega^{\mathrm{f}}, \end{cases} \tag{48}$$

$$0 = \begin{cases} J - 1 & \text{in } \Omega^{\mathrm{s}}, \\ \operatorname{Div}(J\vec{v}\boldsymbol{F}^{-T}) & \text{in } \Omega^{\mathrm{f}}, \end{cases} \tag{49}$$

with the initial conditions

$$\vec{u}(0) = \vec{0} \text{ in } \Omega, \quad \vec{v}(0) = \vec{v}_0 \text{ in } \Omega \tag{50}$$

and boundary conditions

$$\vec{u} = \vec{0}, \quad \vec{v} = \vec{v}_{\mathrm{B}} \text{ on } \Gamma^1, \quad \vec{u} = \vec{0} \text{ on } \Gamma^2, \quad \boldsymbol{\sigma}^{\mathrm{s}}\vec{n} = \vec{0} \text{ on } \Gamma^3. \tag{51}$$

3.2. Constitutive equations

In order to solve the balance equations we need to specify the constitutive relations for the stress tensors. For the fluid we use the incompressible Newtonian relation

$$\boldsymbol{\sigma}^{\mathrm{f}} = -p^{\mathrm{f}}\boldsymbol{I} + \mu(\nabla\vec{v}^{\mathrm{f}} + (\nabla\vec{v}^{\mathrm{f}})^T), \tag{52}$$

where μ represents the viscosity of the fluid and p^{f} is the Lagrange multiplier corresponding to the incompressibility constraint (32).

For the solid part we assume that it can be described by an incompressible hyper-elastic material. We specify the Helmholtz potential Ψ and the solid stress is given by

$$\boldsymbol{\sigma}^{\mathrm{s}} = -p^{\mathrm{s}}\boldsymbol{I} + \varrho^{\mathrm{s}}\frac{\partial \Psi}{\partial \boldsymbol{F}}\boldsymbol{F}^T \tag{53}$$

the first Piola–Kirchhoff stress tensor is then given by

$$\boldsymbol{P}^{\mathrm{s}} = -Jp^{\mathrm{s}}\boldsymbol{F}^{-T} + J\varrho^{\mathrm{s}}\frac{\partial \Psi}{\partial \boldsymbol{F}}, \tag{54}$$

where p^{s} is the Lagrange multiplier corresponding to the incompressibility constraint (43).

The Helmholtz potential can be expressed as a function of different quantities

$$\Psi = \hat{\Psi}(\boldsymbol{F}) = \hat{\Psi}(\boldsymbol{I} + \operatorname{Grad}\vec{u})$$

but due to the principle of material frame indifference the Helmholtz potential Ψ depends on the deformation only through the right Cauchy–Green deformation tensor $\boldsymbol{C} = \boldsymbol{F}^T\boldsymbol{F}$ (see [12])

$$\Psi = \tilde{\Psi}(\boldsymbol{C}). \tag{55}$$

A certain coerciveness condition is usually imposed on the form of the Helmholtz potential

$$\bar{\Psi}(\operatorname{Grad}\vec{u}(\vec{X}, t)) \geqslant a\|\operatorname{Grad}\vec{u}(\vec{X}, t)\|^2 - b(\vec{X}), \tag{56}$$

where a is a positive constant and $b \in L^1(\Omega^s)$. With this assumption and using the integral identity (65) we can derive an energy estimate of the following form

$$\frac{c}{2}\|\vec{v}(T)\|^2_{L^2(\Omega_T)} + \int_0^T \mu\|\nabla\vec{v}\|^2_{L^2(\Omega^f_t)}\,\mathrm{d}t + a\|\mathrm{Grad}\,\vec{u}(T)\|^2_{L^2(\Omega^s)} \leqslant \|b\|_{L^1(\Omega^s)} + \frac{1}{2}\|\vec{v}_0\|^2_{L^2(\Omega^f)} + \frac{\beta}{2}\|\vec{v}_0\|^2_{L^2(\Omega^s)}, \tag{57}$$

where $\beta = \varrho^s/\varrho^f$ and $c = \min(1, \beta)$.

Typical examples for the Helmholtz potential used for isotropic materials like rubber is the Mooney–Rivlin material

$$\tilde{\Psi} = c_1(\mathrm{I}_C - 3) + c_2(\mathrm{II}_C - 3), \tag{58}$$

where $\mathrm{I}_C = \mathrm{tr}\,\boldsymbol{C}$, $\mathrm{II}_C = \mathrm{tr}\,\boldsymbol{C}^2 - \mathrm{tr}^2\boldsymbol{C}$, $\mathrm{III}_C = \det\boldsymbol{C}$ are the invariants of the right Cauchy–Green deformation tensor $\boldsymbol{C}$ and c_i are some material constants. A special case of neo-Hookean material is obtained for $c_2 = 0$. With a suitable choice of the material parameters the entropy inequality and the balance of energy are automatically satisfied.

3.3. Weak formulation

We non-dimensionalize all the quantities by a given characteristic length L and speed V as follows:

$$\hat{t} = t\frac{V}{L}, \quad \hat{\vec{x}} = \frac{\vec{x}}{L}, \quad \hat{\vec{u}} = \frac{\vec{u}}{L}, \quad \hat{\vec{v}} = \frac{\vec{v}}{V},$$

$$\hat{\boldsymbol{\sigma}}^s = \boldsymbol{\sigma}^s\frac{L}{\varrho^f V^2}, \quad \hat{\boldsymbol{\sigma}}^f = \boldsymbol{\sigma}^f\frac{L}{\varrho^f V^2}, \quad \hat{\mu} = \frac{\mu}{\varrho^f V L}, \quad \hat{\Psi} = \Psi\frac{L}{\varrho^f V^2}$$

further using the same symbols, without the hat, for the non-dimensional quantities. The non-dimensionalized system with the choice of material relations, (52) for viscous fluid and (54) for the hyper-elastic solid is

$$\frac{\partial\vec{u}}{\partial t} = \begin{cases} \vec{v} & \text{in } \Omega^s, \\ \Delta\vec{u} & \text{in } \Omega^f, \end{cases} \tag{59}$$

$$\frac{\partial\vec{v}}{\partial t} = \begin{cases} \dfrac{1}{\beta}\,\mathrm{Div}\left(-Jp^s\boldsymbol{F}^{-T} + \dfrac{\partial\Psi}{\partial\boldsymbol{F}}\right) & \text{in } \Omega^s, \\ -(\mathrm{Grad}\,\vec{v})\boldsymbol{F}^{-1}\left(\vec{v} - \dfrac{\partial\vec{u}}{\partial t}\right) + \mathrm{Div}(-Jp^f\boldsymbol{F}^{-T} + J\mu\,\mathrm{Grad}\,\vec{v}\boldsymbol{F}^{-1}\boldsymbol{F}^{-T}) & \text{in } \Omega^f, \end{cases} \tag{60}$$

$$0 = \begin{cases} J - 1 & \text{in } \Omega^s, \\ \mathrm{Div}(J\vec{v}\boldsymbol{F}^{-T}) & \text{in } \Omega^f \end{cases} \tag{61}$$

and the boundary conditions

$$\boldsymbol{\sigma}^f\vec{n} = \boldsymbol{\sigma}^s\vec{n} \text{ on } \Gamma^0_t, \quad \vec{v} = \vec{v}_B \text{ on } \Gamma^1_t, \tag{62}$$

$$\vec{u} = \vec{0} \text{ on } \Gamma^2_t, \quad \boldsymbol{\sigma}^f\vec{n} = \vec{0} \text{ on } \Gamma^3_t. \tag{63}$$

Let $I = [0, T]$ denote the time interval of interest. We multiply the equations (59)–(61) by the test functions $\vec{\zeta}$, $\vec{\xi}$, γ such that $\vec{\zeta} = \vec{0}$ on Γ^2, $\vec{\xi} = \vec{0}$ on Γ^1 and integrate over the space domain Ω and the time interval I. Using integration by

parts on some of the terms and the boundary conditions we obtain

$$\int_0^T \int_\Omega \frac{\partial \vec{u}}{\partial t} \cdot \vec{\zeta} \, \mathrm{d}V \, \mathrm{d}t = \int_0^T \int_{\Omega^s} \vec{v} \cdot \vec{\zeta} \, \mathrm{d}V \, \mathrm{d}t - \int_0^T \int_{\Omega^f} \mathrm{Grad}\, \vec{u} \cdot \mathrm{Grad}\, \vec{\zeta} \, \mathrm{d}V \, \mathrm{d}t, \tag{64}$$

$$\begin{aligned} &\int_0^T \int_{\Omega^f} J \frac{\partial \vec{v}}{\partial t} \cdot \vec{\xi} \, \mathrm{d}V \, \mathrm{d}t + \int_0^T \int_{\Omega^s} \beta J \frac{\partial \vec{v}}{\partial t} \cdot \vec{\xi} \, \mathrm{d}V \, \mathrm{d}t \\ &\quad = -\int_0^T \int_{\Omega^f} J \, \mathrm{Grad}\, \vec{v} \boldsymbol{F}^{-1} \left(\vec{v} - \frac{\partial \vec{u}}{\partial t} \right) \cdot \vec{\xi} \, \mathrm{d}V \, \mathrm{d}t + \int_0^T \int_\Omega J p \boldsymbol{F}^{-T} \cdot \mathrm{Grad}\, \vec{\xi} \, \mathrm{d}V \, \mathrm{d}t \\ &\qquad - \int_0^T \int_{\Omega^s} \frac{\partial \Psi}{\partial \boldsymbol{F}} \cdot \mathrm{Grad}\, \vec{\xi} \, \mathrm{d}V \, \mathrm{d}t - \int_0^T \int_{\Omega^f} J \mu \, \mathrm{Grad}\, \vec{v} \boldsymbol{F}^{-1} \boldsymbol{F}^{-T} \cdot \mathrm{Grad}\, \vec{\xi} \, \mathrm{d}V \, \mathrm{d}t, \end{aligned} \tag{65}$$

$$0 = \int_0^T \int_{\Omega^s} (J-1)\gamma \, \mathrm{d}V \, \mathrm{d}t + \int_0^T \int_{\Omega^f} \mathrm{Div}(J \vec{v} \boldsymbol{F}^{-T}) \gamma \, \mathrm{d}V \, \mathrm{d}t. \tag{66}$$

Let us define the following spaces

$$U = \{\vec{u} \in L^\infty(I, [W^{1,2}(\Omega)]^3), \vec{u} = \vec{0} \text{ on } \Gamma^2\},$$

$$V = \{\vec{v} \in L^2(I, [W^{1,2}(\Omega_t)]^3) \cap L^\infty(I, [L^2(\Omega_t)]^3), \vec{v} = \vec{0} \text{ on } \Gamma^1\},$$

$$P = \{p \in L^2(I, L^2(\Omega))\}$$

then the variational formulation of the fluid-structure interaction problem is stated as follows

Definition 1. Find $(\vec{u}, \vec{v} - \vec{v}_B, p) \in U \times V \times P$ such that Eqs. (64)–(66) are satisfied for all $(\vec{\zeta}, \vec{\xi}, \gamma) \in U \times V \times P$.

3.4. Discretization

In order to solve the problem summarized by Definition 1, we have to create a discrete approximation which can be subsequently solved numerically. The discretization in time is done by the Crank–Nicholson scheme which is only conditionally stable but which has better conservation properties than for example the implicit Euler scheme (see [9,18]). The Crank–Nicholson scheme can be obtained by dividing the time interval I into the series of time steps $[t^n, t^{n+1}]$ with step length $k_n = t^{n+1} - t^n$. Assuming that the test functions are piecewise constant on each time step $[t^n, t^{n+1}]$, $\forall n$, writing the weak formulation (64)–(65) for the time interval $[t^n, t^{n+1}]$, approximating the time derivatives by the central differences

$$\frac{\partial f}{\partial t} \approx \frac{f(t^{n+1}) - f(t^n)}{k_n} \tag{67}$$

and approximating the time integration for the remaining terms by the trapezoidal quadrature rule as

$$\int_{t^n}^{t^{n+1}} f(t) \, \mathrm{d}t \approx \frac{k_n}{2} (f(t^n) + f(t^{n+1})), \tag{68}$$

we obtain the time discretized system. The last equation was taken explicitly for the time t^{n+1} and the corresponding term with the Lagrange multiplier p_h^n in Eq. (65) was also taken explicitly.

3.4.1. 2D space discretization

The discretization in space is done by the finite element method. We approximate the domain Ω by a domain Ω_h with polygonal boundary and by $\mathcal{T}_h$ we denote a set of quadrilaterals covering the domain Ω_h. We assume that $\mathcal{T}_h$ is regular in the sense that any two quadrilateral are disjoint or have a common vertex or a common edge. By $\bar{T} = [-1, 1]^2$ we denote the reference quadrilateral.

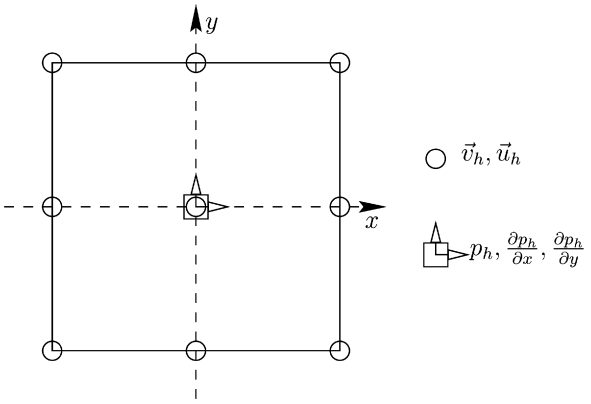

Fig. 3. Location of the degrees of freedom for the Q_2, P_1 element.

Our treatment of the problem as one system suggests we use the same finite elements on both, the solid part and the fluid region. Since both materials are incompressible we have to choose a pair of finite element spaces known to be stable for the problems with incompressibility constraint. One possible choice is the conforming biquadratic, discontinuous bilinear Q_2, P_1 pair, see Fig. 3 for the location of the degrees of freedom.

This choice results in 39 degrees of freedom per element in the case of our displacement, velocity, pressure formulation in two dimensions and 112 degrees of freedom per element in three-dimensions. This seems rather prohibitive, especially for a three-dimensional computation. On the other hand, this choice has quite favorable properties with respect to the accuracy. The computation of the forces on the liquid–solid interface is one of the major difficulties encountered in the classical decoupled methods of solving interaction problems. A comparison of finite volume method, lattice-Boltzmann method and two variants of finite element method with respect to the accuracy of forces evaluation was investigated in [11]. It was shown that the method used here, i.e. the conforming Q_2, P_1 finite element, gives the best results among these methods in terms of achieving given accuracy in force evaluation with the least amount of degrees of freedom. While in our monolithic approach, there is no need for direct stress evaluation at the interface, an accurate stress approximation is still important.

The spaces U, V, P on an interval $[t^n, t^{n+1}]$ would be approximated in the case of Q_2, P_1 pair as

$$U_h = \left\{ \vec{u}_h \in [C(\Omega_h)]^2, \vec{u}_h|_T \in [Q_2(T)]^2 \ \forall T \in \mathscr{T}_h, \vec{u}_h = \vec{0} \text{ on } \Gamma_2 \right\},$$

$$V_h = \left\{ \vec{v}_h \in [C(\Omega_h)]^2, \vec{v}_h|_T \in [Q_2(T)]^2 \ \forall T \in \mathscr{T}_h, \vec{v}_h = 0 \text{ on } \Gamma_1 \right\},$$

$$P_h = \left\{ p_h \in L^2(\Omega_h), p_h|_T \in P_1(T) \ \forall T \in \mathscr{T}_h \right\}.$$

Let us denote by $\vec{u}_h^n$ the approximation of $\vec{u}(t^n)$, $\vec{v}_h^n$ the approximation of $\vec{v}(t^n)$ and p_h^n the approximation of $p(t^n)$. Further we will use following shorthand notation

$$\boldsymbol{F}^n = \boldsymbol{I} + \operatorname{Grad} \vec{u}_h^n, \quad J^n = \det \boldsymbol{F}^n, \quad J^{n+1/2} = \tfrac{1}{2}\left(J^n + J^{n+1}\right),$$

$$(f, g) = \int_\Omega f \cdot g \, \mathrm{d}V, \quad (f, g)_\mathrm{s} = \int_{\Omega^\mathrm{s}} f \cdot g \, \mathrm{d}V, \quad (f, g)_\mathrm{f} = \int_{\Omega^\mathrm{f}} f \cdot g \, \mathrm{d}V,$$

f, g being scalars, vectors or tensors.

Writing down the discrete equivalent of Eqs. (64)–(66) yields

$$\left(\vec{u}_h^{n+1}, \vec{\eta}\right) - \frac{k_n}{2}\left\{\left(\vec{v}_h^{n+1}, \vec{\eta}\right)_\mathrm{s} + \left(\nabla \vec{u}_h^{n+1}, \nabla \vec{\eta}\right)_\mathrm{f}\right\} - \left(\vec{u}_h^n, \vec{\eta}\right) - \frac{k_n}{2}\left\{\left(\vec{v}_h^n, \vec{\eta}\right)_\mathrm{s} + \left(\nabla \vec{u}_h^n, \nabla \vec{\eta}\right)_\mathrm{f}\right\} = 0, \tag{69}$$

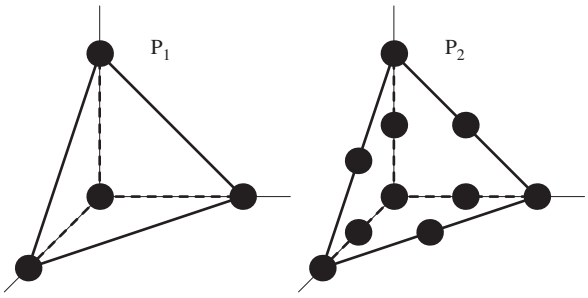

Fig. 4. Location of degrees of freedom for P_1 and P_2.

$$\begin{aligned}
&\left(J^{n+1/2}\vec{v}_h^{n+1},\vec{\xi}\right)_{\mathrm{f}}+\beta\left(\vec{v}_h^{n+1},\vec{\xi}\right)_{\mathrm{s}}-k_n\left(J^{n+1}p_h^{n+1}\left(\boldsymbol{F}^{n+1}\right)^{-T},\operatorname{Grad}\vec{\xi}\right)_{\mathrm{s}}\\
&\quad+\frac{k_n}{2}\left\{\left(\frac{\partial\Psi}{\partial\boldsymbol{F}}\left(\operatorname{Grad}\vec{u}_h^{n+1}\right),\operatorname{Grad}\vec{\xi}\right)_{\mathrm{s}}+\mu\left(J^{n+1}\operatorname{Grad}\vec{v}_h^{n+1}\left(\boldsymbol{F}^{n+1}\right)^{-1},\operatorname{Grad}\vec{\xi}\left(\boldsymbol{F}^{n+1}\right)^{-1}\right)_{\mathrm{f}}\right.\\
&\quad\left.+\left(J^{n+1}\operatorname{Grad}\vec{v}_h^{n+1}\left(\boldsymbol{F}^{n+1}\right)^{-1}\vec{v}_h^{n+1},\vec{\xi}\right)_{\mathrm{f}}\right\}-\frac{1}{2}\left(J^{n+1}\operatorname{Grad}\vec{v}_h^{n+1}\left(\boldsymbol{F}^{n+1}\right)^{-1}\left(\vec{u}_h^{n+1}-\vec{u}_h^{n}\right),\vec{\xi}\right)_{\mathrm{f}}\\
&\quad-\left(J^{n+1/2}\vec{v}_h^{n},\vec{\xi}\right)_{\mathrm{f}}-\beta\left(\vec{v}_h^{n},\vec{\xi}\right)_{\mathrm{s}}+\frac{k_n}{2}\left\{\left(\frac{\partial\Psi}{\partial\boldsymbol{F}}(\operatorname{Grad}\vec{u}_h^{n}),\operatorname{Grad}\vec{\xi}\right)_{\mathrm{s}}+\mu\left(J^{n}\operatorname{Grad}\vec{v}_h^{n}(\boldsymbol{F}^{n})^{-1},\operatorname{Grad}\vec{\xi}(\boldsymbol{F}^{n})^{-1}\right)_{\mathrm{f}}\right.\\
&\quad\left.+\left(J^{n}\operatorname{Grad}\vec{v}_h^{n}(\boldsymbol{F}^{n})^{-1}\vec{v}_h^{n},\vec{\xi}\right)_{\mathrm{f}}\right\}+\frac{1}{2}\left(J^{n}\operatorname{Grad}\vec{v}_h^{n}(\boldsymbol{F}^{n})^{-1}\left(\vec{u}_h^{n+1}-\vec{u}_h^{n}\right),\vec{\xi}\right)_{\mathrm{f}}=0,
\end{aligned}\tag{70}$$

$$\left(J^{n+1}-1,\gamma\right)_{\mathrm{s}}+\left(J^{n+1}\operatorname{Grad}\vec{v}_h^{n+1}\left(\boldsymbol{F}^{n+1}\right)^{-1},\gamma\right)_{\mathrm{f}}=0.\tag{71}$$

Using the basis of the spaces U_h, V_h, P_h as the test functions $\vec{\zeta}$, $\vec{\xi}$, γ we obtain a nonlinear algebraic set of equations. In each time step we have to find $\vec{X}=(\vec{u}_h^{n+1},\vec{v}_h^{n+1},p_h^{n+1})\in U_h\times V_h\times P_h$ such that

$$\vec{\mathscr{F}}(\vec{X})=\vec{0},\tag{72}$$

where $\vec{\mathscr{F}}$ represents system (69)–(71).

3.4.2. Three-dimensional discretization

In the full three-dimensional case the domain Ω is approximated by the polyhedric domain Ω_h, which can be divided into tetrahedrons. By $\mathscr{T}_h$ we will denote the set of all tetrahedrons covering Ω_h. We will assume the regularity of $\mathscr{T}_h$, which means that every two elements are disjoint or have a common face, edge or point. By $\hat{T}$ we will denote the referential element (a tetrahedron with vertices at $[-1,-1,-1]$, $[-1,-1,1]$, $[-1,1,-1]$, $[1,-1,-1]$).

Due to the incompressibility of the materials one has to choose the kind of elements for displacement $\vec{u}$, velocity $\vec{v}$ and pressure p such that the compatibility condition is satisfied. This limits us to certain combinations of elements which we apply to our uniform formulation.

By $P_k(K)$ we will denote polynomials on tetrahedron K of degree $\leqslant k$. We will also need *bubble* functions. These functions for an element K vanish on ∂K. We denote by $B_k(K)$ the space of bubbles that are polynomials of degree less or equal to k on K.

One possible choice, later denoted as *Method* 1 is the P_2,P_1 pair. It is a very common choice and the location of degrees of freedom is shown in Fig. 4. This choice results in 64 degrees of freedom per element (4 for pressure, 10 for one velocity or displacement component) and brings the following discrete version of the spaces U, V, P

on the time interval I_n as

$$\vec{U}_h = \left\{ \vec{\underline{u}}_h \in [C^1(\Omega_h)]^3 : \vec{\underline{u}}_h \lceil_{K_i} \in [P_2(K_i)]^3 \ \forall K_i \in \mathscr{T}_h, \vec{\underline{u}}_h = \vec{0} \text{ on } \Gamma_I, \Gamma_O \right\},$$

$$\vec{V}_h = \left\{ \vec{\underline{v}}_h \in [C^1(\Omega_h)]^3 : \vec{\underline{v}}_h \lceil_{K_i} \in [P_2(K_i)]^3 \ \forall K_i \in \mathscr{T}_h, \vec{\underline{v}}_h = \vec{0} \text{ on } \Gamma_I, \Gamma_O^{\mathrm{s}} \right\},$$

$$P_h = \left\{ \underline{p}_h \in C^0(\Omega_h) : \underline{p}_h \lceil_{K_i} \in P_1(K_i) \ \forall K_i \in \mathscr{T}_h \right\}.$$

The advantage of this choice lies in the easy algorithmic implementation using the barycentrical coordinates, but it requires special care in mesh generation. The corollary of the compatibility condition for this choice gives the following restriction: there cannot exists an element having all vertices on the boundary.

Another possibility, denoted as *Method* 2, is the finite element pair called *minielement*. It consists of taking continuous, piecewise linear functions together with the bubble functions for velocity and continuous, piecewise linear approximation for pressure. This combination has 34 degrees of freedom per element (4 for pressure and 5 for velocity or displacement component). In this case the discrete version of the function spaces is as follows:

$$\vec{U}_h = \left\{ \vec{\underline{u}}_h \in [C^0(\Omega_h)]^3 : \vec{\underline{u}}_h \lceil_{K_i} \in [P_1(K_i) \oplus B_4(K_i)]^3 \ \forall K_i \in \mathscr{T}_h, \vec{\underline{u}}_h = \vec{0} \text{ on } \Gamma_I, \Gamma_O \right\},$$

$$\vec{V}_h = \left\{ \vec{\underline{v}}_h \in [C^0(\Omega_h)]^3 : \vec{\underline{v}}_h \lceil_{K_i} \in [P_1(K_i) \oplus B_4(K_i)]^3 \ \forall K_i \in \mathscr{T}_h, \vec{\underline{v}}_h = \vec{0} \text{ on } \Gamma_I, \Gamma_O^{\mathrm{s}} \right\},$$

$$P_h = \left\{ \underline{p}_h \in C^0(\Omega_h) : \underline{p}_h \lceil_{K_i} \in P_1(K_i) \ \forall K_i \in \mathscr{T}_h \right\}.$$

On tetrahedrons, the local base for velocity is the same as for P_1 plus the product of the barycentrical coordinates. This choice is easy for implementation, it does not require special mesh treatment as the previous method did, but according to our experience this combination without additional stabilization for the convection part is suitable only for lower or at most medium Reynolds number (up to 1200).

3.5. Solution algorithm

System (72) of nonlinear algebraic equations is solved using Newton method as the basic iteration. One step of the Newton iteration can be written as

$$\vec{X}^{n+1} = \vec{X}^n - \left[\frac{\partial \vec{\mathscr{F}}}{\partial \vec{X}} (\vec{X}^n) \right]^{-1} \vec{\mathscr{F}}(\vec{X}^n). \tag{73}$$

The convergence of this basic iteration can reach quadratic rate provided that the initial guess is sufficiently close to the solution. To ensure the convergence globally some improvements of this basic iteration are used.

The damped Newton method with line search improves the chance of convergence by adaptively changing the length of the correction vector. The solution update step in the Newton method (73) is replaced by

$$\vec{X}^{n+1} = \vec{X}^n + \omega \delta \vec{X}, \tag{74}$$

where the parameter ω is found such that certain error measure decreases. One of the possible choices for the quantity to decrease is

$$f(\omega) = \vec{\mathscr{F}}(\vec{X}^n + \omega \delta \vec{X}) \cdot \delta \vec{X}. \tag{75}$$

Since we know

$$f(0) = \vec{\mathscr{F}}(\vec{X}^n) \cdot \delta \vec{X} \tag{76}$$

and

$$f'(0) = \left[\frac{\partial \vec{\mathscr{F}}}{\partial \vec{X}} (\vec{X}^n) \right] \delta \vec{X} \cdot \delta \vec{X} = \vec{\mathscr{F}}(\vec{X}^n) \cdot \delta \vec{X} \tag{77}$$

(1) Let $\vec{X}^n$ be some starting guess.
(2) Set the residuum vector $\vec{R}^n = \vec{\mathscr{F}}(\vec{X}^n)$ and the tangent matrix $\boldsymbol{A} = \frac{\partial \vec{\mathscr{F}}}{\partial \vec{X}}(\vec{X}^n)$.
(3) Solve for the correction $\delta\vec{X}$

$$\boldsymbol{A}\delta\vec{X} = \vec{R}^n.$$

(4) Find optimal step length ω.
(5) Update the solution $\vec{X}^{n+1} = \vec{X}^n - \omega\delta\vec{X}$.

Fig. 5. One step of the Newton method with the line search.

and computing $f(\omega_0)$ for $\omega_0 = -1$ or ω_0 determined adaptively from previous iterations we can approximate $f(\omega)$ by a quadratic function

$$f(\omega) = \frac{f(\omega_0) - f(0)(\omega_0 + 1)}{\omega_0^2}\omega^2 + f(0)(\omega + 1). \tag{78}$$

Then setting

$$\tilde{\omega} = \frac{f(0)\omega_0^2}{f(\omega_0) - f(0)(\omega_0 + 1)}, \tag{79}$$

the new optimal step length $\omega \in [-1, 0]$ is

$$\omega = \begin{cases} -\dfrac{\tilde{\omega}}{2} & \text{if } \dfrac{f(0)}{f(\omega_0)} > 0, \\ -\dfrac{\tilde{\omega}}{2} - \sqrt{\dfrac{\tilde{\omega}^2}{4} - \tilde{\omega}} & \text{if } \dfrac{f(0)}{f(\omega_0)} \leqslant 0. \end{cases} \tag{80}$$

This line search can be repeated with ω_0 taken as the last ω until, for example, $f(\omega) \leqslant \frac{1}{2} f(0)$. By this we can enforce a monotonous convergence of the approximation $\vec{X}^n$ (Fig. 5).

An adaptive time-step selection was found to help in the nonlinear convergence. A heuristic algorithm was used to correct the time-step length according to the convergence of the nonlinear iterations in the previous time-step. If the convergence was close to quadratic, i.e. only up to three Newton steps were needed to obtain required precision, the time step could be slightly increased, otherwise the time-step length was reduced.

The structure of the Jacobian matrix $\partial\vec{\mathscr{F}}/\partial\vec{X}$ is

$$\frac{\partial \vec{\mathscr{F}}}{\partial \vec{X}}(\vec{X}) = \begin{pmatrix} A_{vv} & A_{vu} & B_v \\ A_{uv} & A_{uu} & B_u \\ B_v^T & B_u^T & 0 \end{pmatrix} \tag{81}$$

and it can be computed by finite differences from the residual vector $\vec{\mathscr{F}}(\vec{X})$

$$\left[\frac{\partial \vec{\mathscr{F}}}{\partial \vec{X}}\right]_{ij}(\vec{X}^n) \approx \frac{[\vec{\mathscr{F}}]_i(\vec{X}^n + \alpha_j \vec{e}_j) - [\vec{\mathscr{F}}]_i(\vec{X}^n - \alpha_j \vec{e}_j)}{2\alpha_j}, \tag{82}$$

where $\vec{e}_j$ are the unit basis vectors in $\mathbb{R}^n$ and coefficients α_j are adaptively taken according to the change in the solution in the previous time step. Since we know the sparsity pattern of the Jacobian matrix in advance, it is given by the used finite element method, this computation can be done in an efficient way so that the linear solver remains the dominant part in terms of the cpu time.

The linear problems are solved by BiCGStab iterations with ILU preconditioner with allowed certain fill-in for the diagonal blocks. The algorithms used are described in [3] and the implementation was taken from [4].

4. Mixture model formulation

In this section we formulate and propose a solution algorithm for a steady state, two-dimensional problem of a stretched rectangular slab of solid–fluid mixture. Two or three-dimensional problems for solid–fluid mixtures in connection with hydrated biological tissue were recently presented in [39,38,40,8,44,1] for a biphasic mixture to model behavior of articular cartilage under compression. In all these works the nonlinear and unsteady inertia of the fluid is neglected.

4.1. Model formulation

We consider a model for steady perfusion within a mixture slab introduced for example in [34]. Let $\vec{u}$ denote the solid displacement, $\vec{v} = \vec{v}^{\mathrm{f}}$ denotes the fluid velocity while $\vec{v}^{\mathrm{s}} = \vec{0}$ due to the assumption of a steady state, ϕ is the fluid volume fraction and p is the Lagrange multiplier associated with the incompressibility constraint. The interaction between the elastic material and the perfusing fluid is realized by the drag force in the form

$$\alpha\phi(1-\phi)(\vec{v}^{\mathrm{f}} - \vec{v}^{\mathrm{s}}) \tag{83}$$

which in the case of steady solution reduces to $\alpha\phi(1-\phi)\vec{v}$.

Our task is to find $(\vec{u}, \vec{v}, \phi, p)$ such that

$$\phi(\nabla\vec{v})\vec{v} + \nabla p - \operatorname{div}\boldsymbol{\sigma}^{\mathrm{s}} = 0, \tag{84}$$

$$(\nabla\vec{v})\vec{v} + \nabla(p+\Psi) - \operatorname{div}\boldsymbol{\sigma}^{\mathrm{f}} + (1-\phi)\boldsymbol{\alpha}\vec{v} = 0, \tag{85}$$

$$(1-\phi)\det\boldsymbol{F} = \phi_0^{\mathrm{s}}, \tag{86}$$

$$\operatorname{div}(\phi\vec{v}) = 0 \tag{87}$$

holds in domain Ω, where ϕ_0^{s} is the volume fraction of the solid in the reference state and the Helmholtz potential Ψ is given by constitutive equation as a function of ϕ and $\boldsymbol{F}$. The Cauchy stress tensor $\boldsymbol{\sigma}^{\mathrm{s}}$ is then given by

$$\boldsymbol{\sigma}^{\mathrm{s}} = (\phi + \beta(1-\phi))\frac{\partial\Psi}{\partial\boldsymbol{F}}\boldsymbol{F}^T, \tag{88}$$

where $\beta = \varrho_t^{\mathrm{s}}/\varrho_t^{\mathrm{f}}$ is the true mass ratio. By $\boldsymbol{S}$ we will denote the Piola–Kirchoff stress tensor

$$\boldsymbol{S} = -p(\det\boldsymbol{F})\boldsymbol{F}^{-T} + (\phi + \beta(1-\phi))(\det\boldsymbol{F})\frac{\partial\Psi}{\partial\boldsymbol{F}}. \tag{89}$$

Let the boundary $\partial\Omega$ be divided into three disjoint parts $\partial\Omega = \bigcup_{i=1}^{3}\Gamma_i$. Let $\vec{n}$ be the unit normal vector to the boundary $\partial\Omega$. Then if $\vec{t}$ is given traction on the boundary, $\vec{u}_{\mathrm{B}}$ is given solid boundary displacement and $\vec{v}_{\mathrm{B}}$ is given fluid velocity at the boundary the possible boundary conditions are

$$\tfrac{1}{3}\operatorname{tr}\boldsymbol{\sigma} = p_{\mathrm{B}}, \quad \vec{u} = \vec{u}_{\mathrm{B}} \quad \text{on } \Gamma_1, \tag{90}$$

$$-p\vec{n} + \boldsymbol{\sigma}^{\mathrm{s}}\vec{n} = \vec{t}, \quad \vec{v} = \vec{v}_{\mathrm{B}} \quad \text{on } \Gamma_2, \tag{91}$$

$$\vec{u} = \vec{u}_{\mathrm{B}}, \quad \vec{v} = \vec{v}_{\mathrm{B}} \quad \text{on } \Gamma_3. \tag{92}$$

We avoid prescribing partial stresses on the boundary since it is not clear weather such values can be obtained by measurements or how it should be partitioned into the partial stresses. Instead, we focus on the prescription of the fluid velocity at the boundary. There are other possible boundary conditions, apart of prescribing the fluid velocity. We may prescribe

$$\phi\vec{v} = \vec{f}_{\mathrm{B}} \tag{93}$$

or the total fluid flux through certain part of the boundary

$$\int_{\Gamma}\phi\vec{v}\cdot\vec{n}\,\mathrm{d}a = f_{\mathrm{B}} \tag{94}$$

which would be convenient as an outflow boundary condition. On the other hand the implementation of these conditions in the solution process is more complicated.

4.2. Weak formulation

In order to apply the finite element method we formulate our problem in a weak sense. Let us define spaces U, V, M and P as follows:

$$U = \left\{ \vec{u} \in [W^{1,2}(\Omega^s)]^2, \vec{u} = \vec{0} \text{ on } \Gamma_1 \cup \Gamma_3 \right\}, \tag{95}$$

$$V = \left\{ \vec{v} \in [W^{1,2}(\Omega^s)]^2, \vec{v} = 0 \text{ on } \Gamma_2 \cup \Gamma_3 \right\}, \tag{96}$$

$$M = \left\{ \phi \in W^{1,2}(\Omega^s) \right\}, \tag{97}$$

$$P = \left\{ p \in L^2(\Omega^s) \right\}. \tag{98}$$

Multiplying Eqs. (84)–(87) by a test functions $(\vec{\zeta}, \vec{\xi}, \eta, \gamma)$, integrating over the domain Ω and transforming the integration to the reference domain Ω^s yields

$$\int_{\Omega^s} \phi \nabla \vec{v} \operatorname{cof} \boldsymbol{F}^T \vec{v} \cdot \vec{\zeta} \, \mathrm{d}X - \int_{\Omega^s} p \operatorname{cof} \boldsymbol{F} \cdot \nabla \vec{\zeta} \, \mathrm{d}X + \int_{\Omega^s} \boldsymbol{S}^E \cdot \nabla \vec{\zeta} \, \mathrm{d}X - \int_{\Gamma_2} \vec{t} \operatorname{cof} \boldsymbol{F} \vec{N} \cdot \vec{\zeta} \, \mathrm{d}A = 0, \tag{99}$$

$$\begin{aligned} &\int_{\Omega^s} \nabla \vec{v} \operatorname{cof} \boldsymbol{F} \vec{v} \cdot \vec{\xi} \, \mathrm{d}X - \int_{\Omega^s} (p + \Psi) \operatorname{cof} \boldsymbol{F} \cdot \nabla \vec{\xi} \, \mathrm{d}X + \int_{\Omega^s} (1 - \phi) \boldsymbol{\alpha} \vec{v} \cdot \vec{\xi} \det \boldsymbol{F} \, \mathrm{d}X \\ &\quad + \int_{\Gamma_1} \left(p_B - \frac{1}{3} \operatorname{tr} \boldsymbol{\sigma} + \Psi \right) \operatorname{cof} \boldsymbol{F} \vec{N} \cdot \vec{\xi} \, \mathrm{d}A = 0, \end{aligned} \tag{100}$$

$$\int_{\Omega^s} ((1 - \phi) \det \boldsymbol{F} - \phi_0^s) \eta \, \mathrm{d}X = 0, \tag{101}$$

$$\int_{\Omega^s} \nabla(\phi \vec{v}) \cdot \operatorname{cof} \boldsymbol{F} \gamma \, \mathrm{d}X = 0, \tag{102}$$

where $\operatorname{cof} \boldsymbol{F} = \det \boldsymbol{F} \boldsymbol{F}^{-T}$ and the inner product for two tensors is defined as $\boldsymbol{F} \cdot \boldsymbol{G} = \operatorname{tr}(\boldsymbol{F}^T \boldsymbol{G})$. Then our task is to find $(\vec{u}, \vec{v}, \phi, p)$ such that $(\vec{u} - \vec{u}_B, \vec{v} - \vec{v}_B, \phi, p) \in U \times V \times M \times P$ and Eqs. (99)–(102) are satisfied for all $(\vec{\zeta}, \vec{\xi}, \eta, \gamma) \in U \times V \times M \times P$.

4.3. Discretization

We apply the same discretization and solution technique as in the previous section. The reference domain Ω^s is approximated by a domain Ω_h with piecewise linear boundary. The interior is divided by regular quadrilateral mesh into convex quadrilateral elements. The set of all quadrilaterals in Ω_h is denoted by $\mathscr{T}_h$ and $\tilde{T} = (-1, 1)^2$ is the reference quadrilateral. For each element $T \in \mathscr{T}_h$ there is a bilinear one to one mapping on to the reference element $\tilde{T}$. The spaces U, V, M and P are approximated respectively by the following finite element spaces

$$U_h = \left\{ \vec{u}_h \in [C(\Omega_h)]^2, \vec{u}_h / T \in [Q_2(T)]^2 \ \forall T \in \mathscr{T}_h, \vec{u}_h = \vec{0} \text{ on } \Gamma_1 \cup \Gamma_3 \right\}, \tag{103}$$

$$V_h = \left\{ \vec{v}_h \in [C(\Omega_h)]^2, \vec{v}_h / T \in [Q_2(T)]^2 \ \forall T \in \mathscr{T}_h, \vec{v}_h = 0 \text{ on } \Gamma_1 \cup \Gamma_3 \right\}, \tag{104}$$

$$M_h = \left\{\phi_h \in C(\Omega_h),\, \phi_h/T \in Q_1(T)\ \forall T \in \mathcal{T}_h,\, 0 \leqslant \phi_h \leqslant 1\right\}, \tag{105}$$

$$P_h = \{p_h \in C(\Omega_h),\, p_h/T \in Q_1(T)\ \forall T \in \mathcal{T}_h\}. \tag{106}$$

The resulting discrete problem is obtained by taking the usual nodal basis of the space $U_h \times V_h \times M_h \times P_h$ and using the elements of this basis as test functions $(\vec{\zeta}, \vec{\xi}, \eta, \gamma)$ in (99)–(102). This set of nonlinear algebraic equations can be written as

$$\vec{\mathcal{F}}(\vec{X}) = \vec{0}, \tag{107}$$

where $\vec{X} = (\vec{u}_h, \vec{v}_h, \phi_h, p_h)$ is the vector of unknown components.

The Jacobian matrix $[\partial\vec{\mathcal{F}}/\partial\vec{X}(\vec{X})]$ has following structure

$$\left[\frac{\partial\vec{\mathcal{F}}}{\partial\vec{X}}(\vec{X})\right] = \begin{pmatrix} \boldsymbol{A}_{u,u} & \boldsymbol{A}_{u,v} & \boldsymbol{B}_{u,\phi} & \boldsymbol{C} \\ \boldsymbol{A}_{v,u} & \boldsymbol{A}_{v,v} & \boldsymbol{B}_{v,\phi} & \boldsymbol{C} \\ (1-\phi)\boldsymbol{C}^T & \boldsymbol{0} & \boldsymbol{B}_{\phi,\phi} & \boldsymbol{0} \\ \boldsymbol{A}_{p,u} & \phi\boldsymbol{C}^T & \boldsymbol{B}_{p,\phi} & \boldsymbol{0} \end{pmatrix}. \tag{108}$$

This matrix has the typical structure of a constraint system with zero diagonal block.

4.4. Solution algorithm

System (107) of nonlinear algebraic equations is again solved using the same approach like in the previous section. Additionally, since we seek the steady solution in this case, the continuation method is employed in order to have the starting approximation in the Newton iteration in the range of convergence. In the continuation method the problem $\vec{F}(\vec{X}) = 0$ is replaced by

$$\vec{G}(\vec{X}, \lambda) = 0, \tag{109}$$

where λ is a parameter such that for $\vec{G}(\vec{X}, 0) = 0$ we know the solution, while for $\lambda = 1$ the original problem is recovered

$$\vec{G}(\vec{X}, 1) \equiv \vec{F}(\vec{X}). \tag{110}$$

For example, one can make the boundary conditions depend on the parameter λ in such a way that for $\lambda = 0$ we have the undeformed, stress free state, and for $\lambda = 1$ we have the original boundary conditions.

In the process of the continuation method, we follow the solution curve given by the initial value problem

$$\frac{\mathrm{d}}{\mathrm{d}s}\vec{G}(\vec{X}(s), \lambda(s)) = 0, \tag{111}$$

$$(\vec{X}(0), \lambda(0)) = (\vec{X}_0, 0), \tag{112}$$

until the point $\lambda(s) = 1$. The basic method used to solve this problem is the Euler–Newton iteration, outlined in Fig. 6, where the explicit Euler method is applied to (111) as predictor and then the solution is corrected by the Newton method. This step is repeated until $\lambda^n = 1$. The parameter ω in the update step can be fixed or can be chosen adaptively, for example depending on the number of Newton iterations in the correction step needed to correct the solution.

The Jacobian matrix is computed again via finite differences. To invert the matrices in the most inner loops, BiCGStab or GMRES methods are used with preconditioning. See [2–4] for further details on these methods. The incomplete LU decomposition is used for preconditioning with suitable ordering of the unknowns and with fill-in allowed for certain pattern in the zero diagonal block of the Jacobian matrix.

5. Applications

In this section we present a few example applications to demonstrate the presented methods. As a motivation we consider the possible numerical simulation of some problems encountered in the area of cardiovascular hemodynamics,

(1) Let $\vec{X}^n$ be given starting approximation and λ^n the value of the continuation parameter.
(2) Predictor step. Solve for $(\dot{\vec{X}}^n, \dot{\lambda}^n)$

$$\left[\frac{\partial \vec{G}}{\partial \vec{X}}(\vec{X}^n, \lambda^n)\right] \dot{\vec{X}}^n + \left[\frac{\partial \vec{G}}{\partial \lambda}(\vec{X}^n, \lambda^n)\right] \dot{\lambda}^n = 0, \tag{113}$$

$$\|(\dot{\vec{X}}^n, \dot{\lambda}^n)\| = 1. \tag{114}$$

(3) Update the solution $(\vec{X}^{n+\frac{1}{2}}, \lambda^{n+1}) = (\vec{X}^n, \lambda^n) + \omega(\dot{\vec{X}}^n, \dot{\lambda}^n)$.
(4) Correction step. Solve for $\vec{X}^{n+1}$ by Newton iteration with $\vec{X}^{n+\frac{1}{2}}$ as starting guess

$$\vec{G}(\vec{X}^{n+1}, \lambda^{n+1}) = 0. \tag{115}$$

Fig. 6. One step of Euler–Newton algorithm.

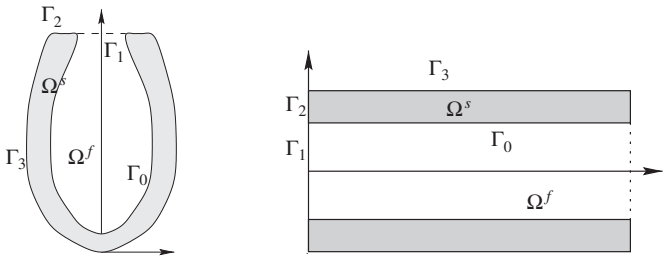

Fig. 7. Schematic view of the ventricle and elastic tube geometries.

namely flow interaction with thick-walled deformable material, which can become a useful tool for deeper understanding of the onset of diseases of the human circulatory system, as for example blood cell and intima damages in stenosis, aneurysm rupture, evaluation of the new surgery techniques of heart, arteries and veins.

In order to test the proposed numerical methods, a simplified two- and three-dimensional examples which include interaction of flow with deformable material are computed. The first example is a flow in an ellipsoidal cavity and the second is a flow through a channel with elastic walls and three-dimensional example of simple thick wall breathalyzer. In all cases the flow is driven by changing fluid pressure at the inflow part of the boundary while the elastic part of the boundary is either fixed or stress free.

The constitutive relations used for the materials are the incompressible Newtonian model (52) for the fluid and the hyper-elastic neo-Hookean material (58) with $c_2 = 0$ for the solid. This choice includes all the main difficulties the numerical method has to deal with, namely the incompressibility and large deformations.

5.1. Flow in an ellipsoidal cavity

The motivation for our first test is the left heart ventricle which is an approximately ellipsoidal chamber surrounded by the heart muscle. In our two-dimensional computations we use an ellipsoidal cavity, see Fig. 7, with prescribed time-dependent natural boundary condition at the fluid boundary part Γ^1

$$p(t) = \sin t \quad \text{on } \Gamma^1. \tag{116}$$

The material of the solid wall is modeled by the simple neo-Hookean constitutive relation (58) with $c_2 = 0$.

Figs. 8 and 9 show the computational grid for the maximal and minimal volume configuration of the cavity and the velocity field of the fluid for the same configurations. One of the important characteristics is the shear stress exerted by the fluid flow on the wall material. Fig. 9 shows the distribution of the shear stress in the domain for three different

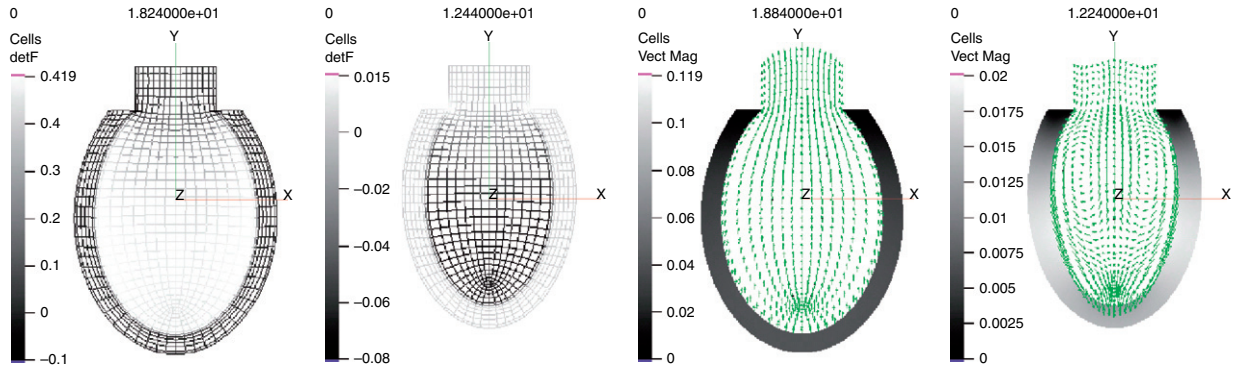

Fig. 8. Maximum and minimum volume configuration with the fluid flow.

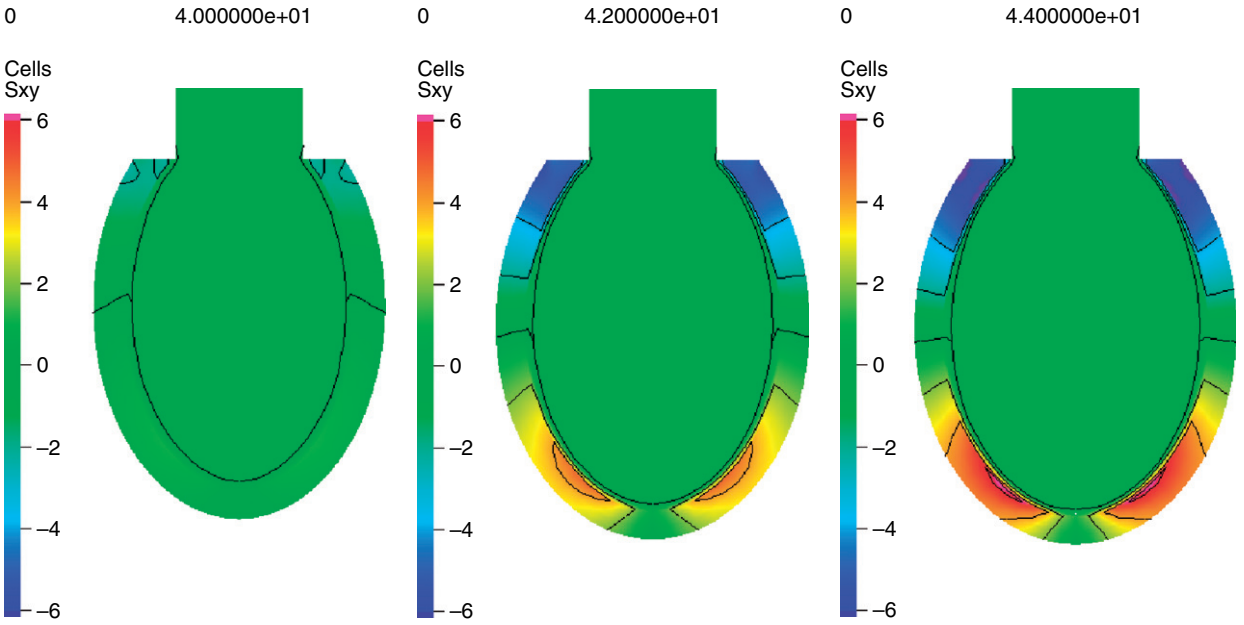

Fig. 9. Shear stress distribution in the wall during the period.

times. In Figs. 10 and 11 the volume change of the cavity as a function of the time and the average pressure inside the cavity versus the volume of the cavity is shown together with the trajectory and velocity of a material point on the solid–fluid interface. We can see that after the initial cycle which was started from the undeformed configuration the system comes to a time periodic solution.

5.2. Flow in an elastic channel

The second example application is the simulation of a flow between elastic plates. The plates are fixed at both ends, stress free boundary condition is applied on their outer sides, and the flow is driven by a time-dependent pressure difference between the ends of the channel of the form (116). For the flow in the channel without any constriction the time dependence of the fluid volume inside the channel is shown together with the pressure volume diagram in the figure and the trajectory and velocity of a material point on the solid–fluid interface in Figs. 13 and 14. The velocity field is shown in Fig. 12 at different stages of the pulse. Figs. 12–14.

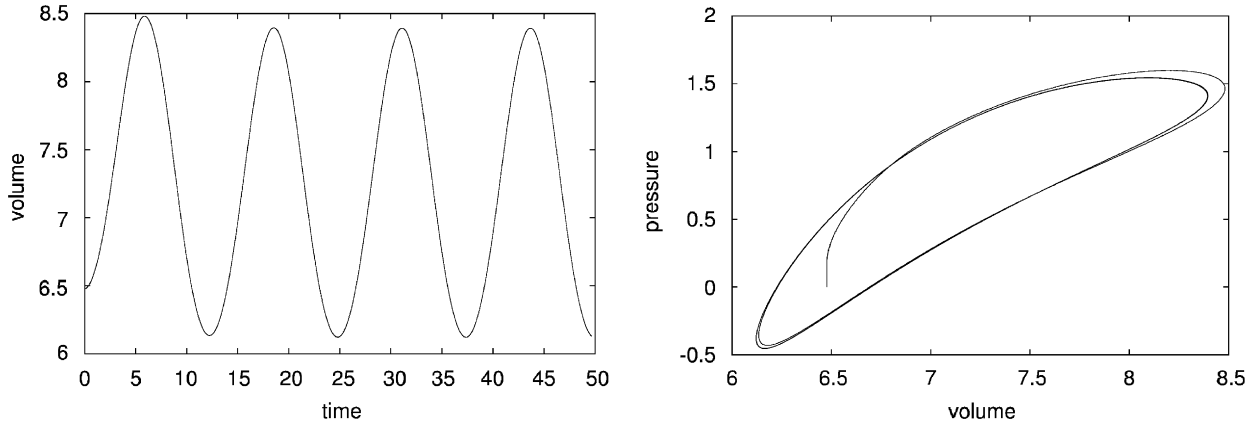

Fig. 10. Volume of the fluid inside and the pressure-volume diagram for the ellipsoidal cavity test.

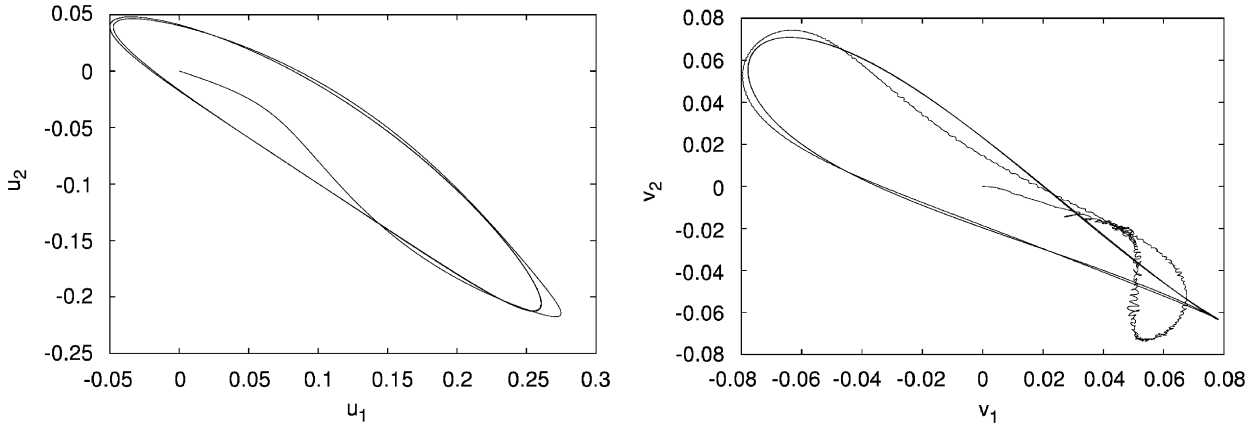

Fig. 11. The displacement trajectory and velocity of a point at the fluid solid interface (inner side of the wall) for the ellipsoidal cavity test.

Such flow is also interesting to investigate in the presence of some constriction as a valve flap, blood clot or stenosis. Such configuration is shown in Fig. 15 where again a time dependent pressure difference between the ends of the channel creates a flow between the two elastic walls with short flap attached to the bottom wall. Fig. 15 shows the velocity field in the fluid and the pressure distribution throughout the wall for the computation of the flow in a channel with elastic obstruction. In this example the elastic obstruction is modeled by the same material as the walls of the channel. Both ends of the walls are fixed at the inflow and outflow and the flow is again driven by a periodic change of the pressure at the left end.

5.3. Three-dimensional model of breathalyzer

The results presented here try to demonstrate the potential possibilities of our method when extended to three-dimensional as described in Section 3.4.2. For each example we present a three-dimensional view of the grid with related computational parameters, and the main results are shown in sectorial views. The cpu time of each computation was measured on a computer with Intel P4 2.8 GHz processor and 1 GB RAM. The program Netgen was used to generate the mesh and all results were visualized by the program Tecplot.

As an example of a fluid-structure problem we have chosen a breathalyzer (see Fig. 16). This rubber-like children toy helps us to test our three-dimensional approach. At Fig. 17 there is the undeformed state of a solid thin layer, the fluid, and the initial pressure distribution.

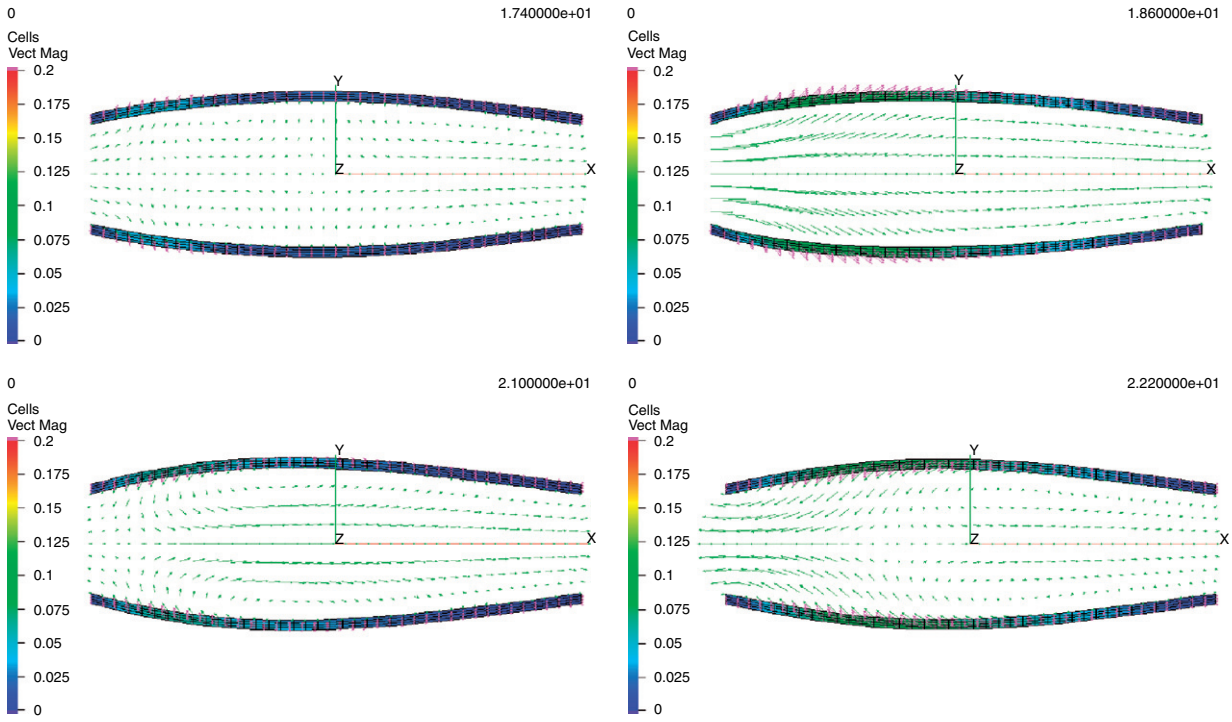

Fig. 12. Velocity field during one pulse in channel without an obstacle.

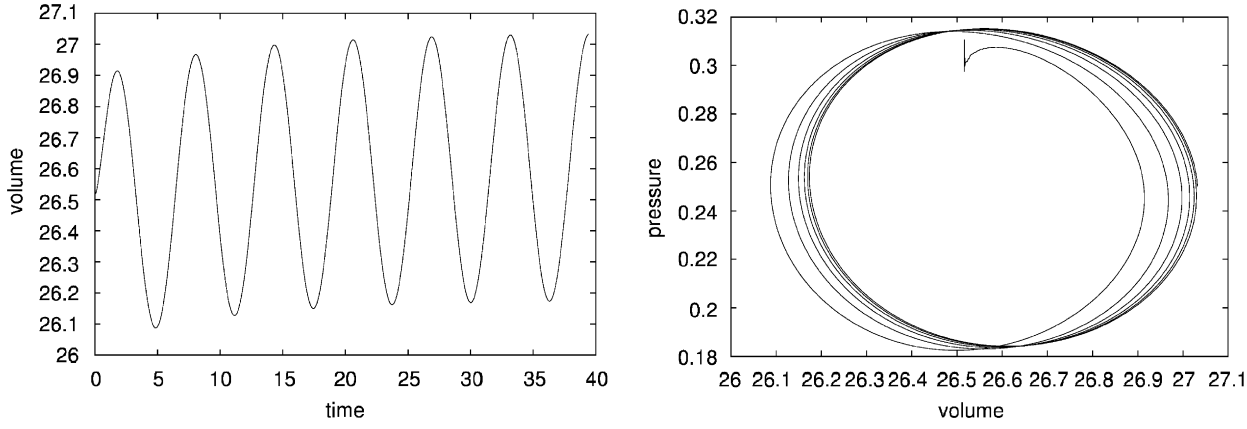

Fig. 13. Volume of the fluid in the channel and the pressure-volume diagram.

The first example is a simulation of exhausting the breathalyzer. The balloon is modeled as a neo-Hookean material and the density ratio β is set to 1000. We prescribe the fluid velocity profile in the direction of the outer normal to the boundary Γ_O^{f} (it is the only active boundary condition; on the other parts zero Neumann condition is prescribed). After 11 s of real time the computation stops due to a partial collapse of the outlet tube (see Fig. 18). We can again see the solid and the fluid parts separately, and also the pressure distribution.

The simulation of the reverse process is another example. We start again with the undeformed state at Fig. 17, change the direction of velocity, and thus change the output to input. After approximately 10 s of real time the computation stops. The last presentable configuration is at Fig. 19—again presenting separately the solid and the fluid parts, and pressure distribution in a sectorial view.

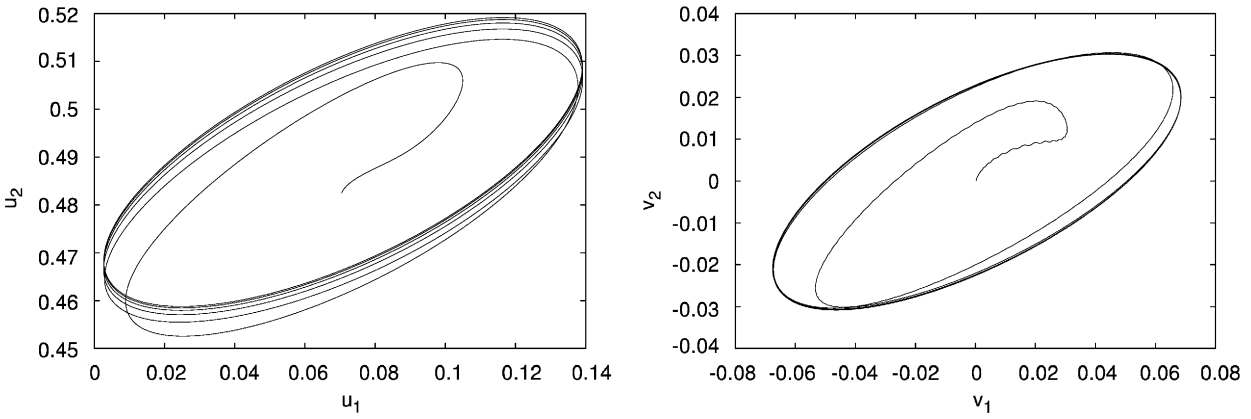

Fig. 14. Displacement trajectory and velocity of a point at the fluid solid interface (inner side of the wall).

5.4. Illustrative example of perfusion

Motivated by [15], where a one-dimensional version of this kind of example was used for the material identification, we consider a simple biaxial deformation of a soft tissue speciment. Such a simple deformation can provide useful hints for experiments with biological tissues or together with the experimental data it can be used to identify the values of the material parameters of the constitutive law. In such cases the fluid part of the mixture diffuses with speed dictated by biological conditions, e.g. blood flow in capillaries, for which the inertial effects might be significant.

We take two-dimensional crossection of the slab along the direction of the perfusion. Let $\Omega^{\mathrm{s}} = [-L, L] \times [-H, H] \times [-L, L]$ be the reference domain occupied by the solid. The deformed domain, shown in Fig. 20, is

$$\Omega = \{x = X + \vec{u}(X), \forall X \in \Omega^{\mathrm{s}}\}. \tag{117}$$

The deformation is assumed to be of a form

$$x_1 = X_1 + u_1(X_1, X_2), \quad x_2 = X_2 + u_2(X_1, X_2), \quad x_3 = \lambda_3 X_3, \tag{118}$$

where λ_3 is prescribed positive constant. The fluid velocity is assumed to be

$$\vec{v}(x_1) = (v_1(x_1, x_2), v_2(x_1, x_2), 0). \tag{119}$$

The constitutive relation for the Helmholtz potential is used in the form

$$\Psi = c_1(\mathrm{I}_C - 3) + c_2 \ln(\phi). \tag{120}$$

The boundary conditions applied are $\boldsymbol{\sigma}\vec{n} = \vec{t}$, $\phi\vec{v} = \vec{v}_{\mathrm{B}}$ at the left end of the speciment, $u_1 = 0$, $\sigma_{12} = 0$, $\frac{1}{3}\operatorname{tr}\boldsymbol{\sigma} = p_{\mathrm{B}}$ at the right end and $\boldsymbol{\sigma}\vec{n} = \vec{0}$, $\phi\vec{v} = \vec{v}_{\mathrm{B}}$ the top and bottom boundaries.

In Fig. 21 is shown the finite element grid on the reference configuration of the solid. The initial solution is taken to be zero displacement and velocity, given constant volume fraction and Lagrange multiplier p such that the solution is stress free. The solution for required values of the boundary conditions is computed by continuation. In Fig. 21 the finite element grid on the deformed configuration of the solid is shown. We can see that the slab becomes thicker in the X_2 direction at the left end, and thinner at the fluid outflow end. This variation in the thickness is caused by the gradual decrease in the pressure along the fluid flow. Fig. 22 shows the velocity field of the perfusion and the fluid volume fraction throughout the slab. The fluid velocity increases toward the end of the slab while the volume fraction decreases. In Fig. 23 the pressure field is shown together with the stress tensor components. We can note the presence of stress concentration around the corners of the slab where the type of the boundary condition changes.

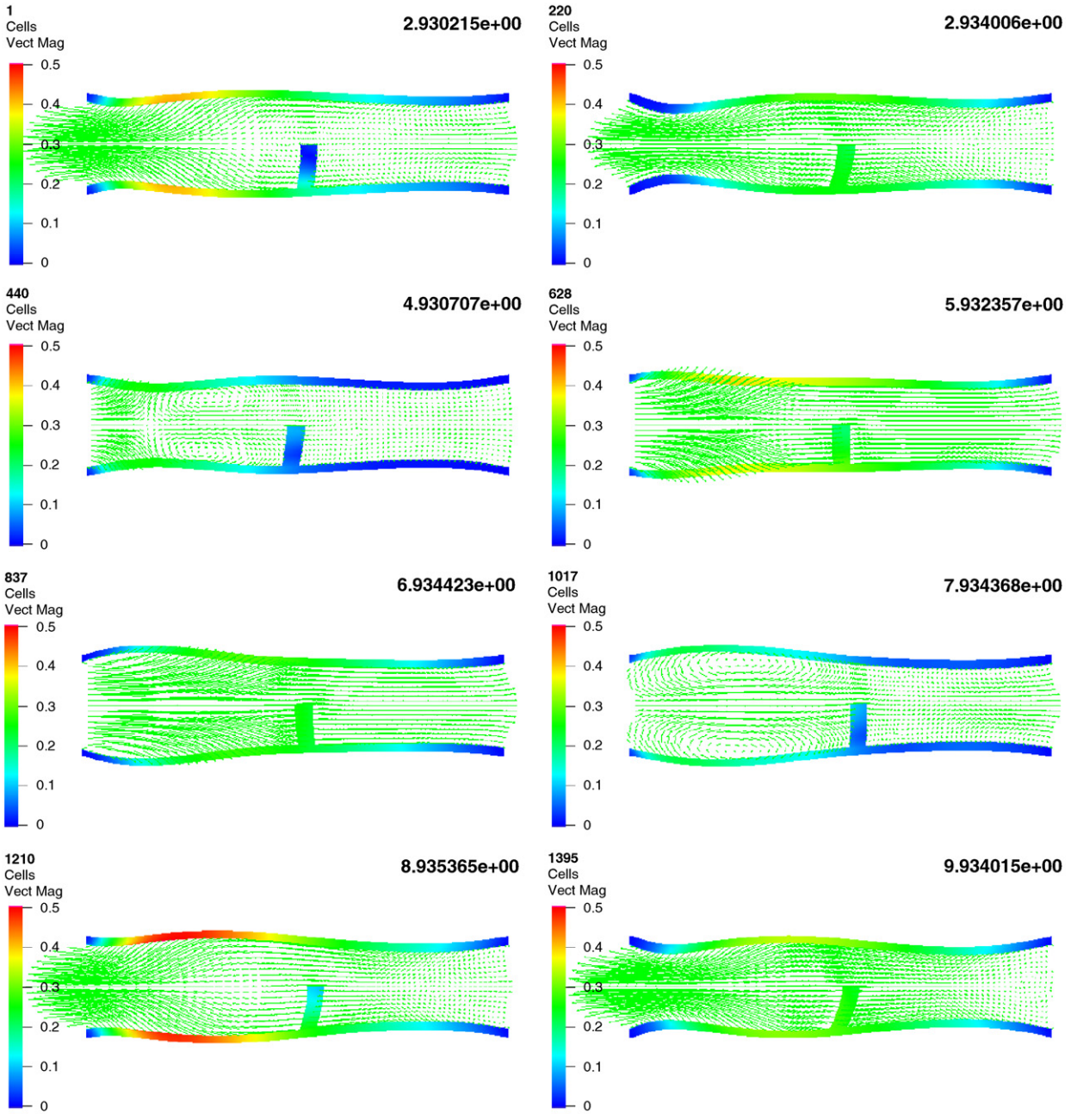

Fig. 15. Fluid flow and pressure distribution in the wall during one pulse for the example flow in a channel with constriction.

6. Summary and future development

In this paper we present a general formulation of dynamic fluid-structure interaction problem suitable for applications with finite deformations and laminar flows. While the presented example calculations are simplified to allow initial testing of the numerical methods the formulation is general enough to allow immediate extension to more realistic material models. For example in the case of material anisotropy one can consider

$$\tilde{\Psi} = c_1(\mathrm{I}_C - 3) + c_2(\mathrm{II}_C - 3) + c_3(|\boldsymbol{F}\vec{a}| - 1)^2,$$

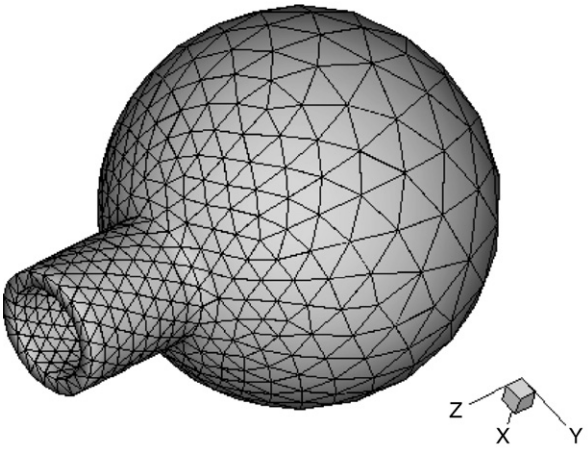

Elements	6 508
Equations	48 771
Comp time	5 days
Time iters	1154
μ	0.1
β	1000
θ	0.5
Material	neo-Hookean
FEM	Method 2

Fig. 16. Breathalyzer—grid view.

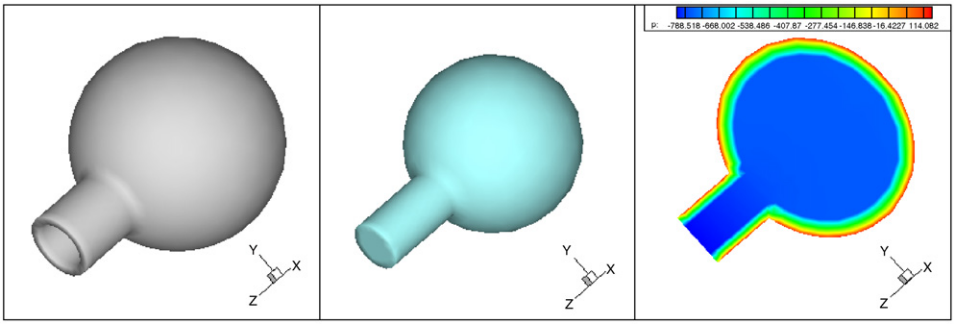

Fig. 17. The breathalyzer—initial state.

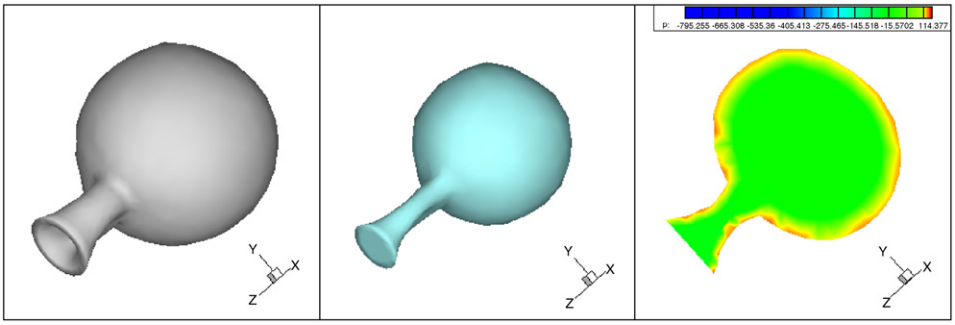

Fig. 18. The blowing out of breathalyzer—final state.

with $\vec{a}$ being the preferred material direction. The term $|\boldsymbol{F}\vec{a}|$ represents the extension in the direction $\vec{a}$. In [16,17] a similar material relation of the form

$$\tilde{\Psi} = c_1(\exp(b_1(\mathrm{I}_C - 3)) - 1) + c_2(\exp(b_2(|\boldsymbol{F}\vec{a}| - 1)) - 1)$$

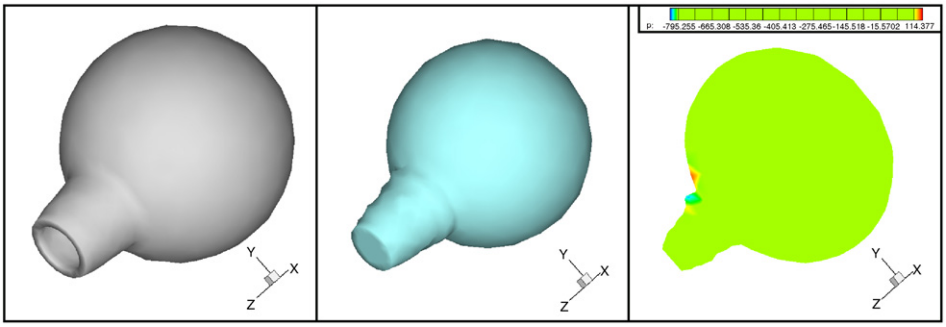

Fig. 19. The inflation of breathalyzer—final state.

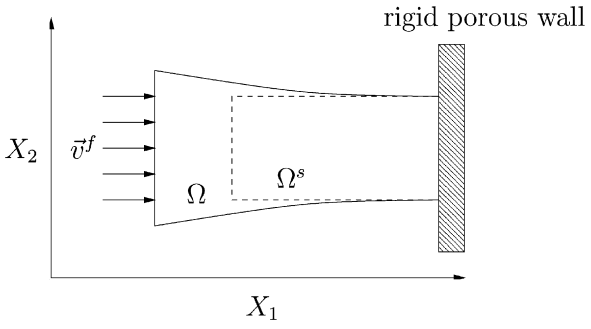

Fig. 20. Undeformed and deformed configuration in two dimensional perfusion problem.

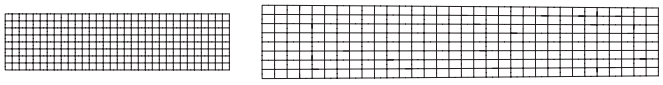

Fig. 21. Finite element grid on the reference and the deformed configuration of the solid.

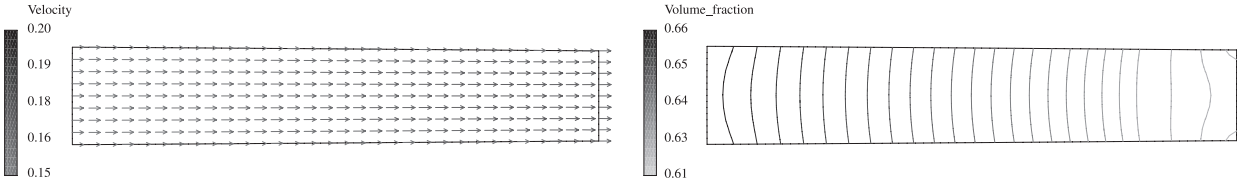

Fig. 22. Fluid velocity and the fluid volume fraction.

has been proposed to describe passive behavior of muscle tissue. Adding to any form of Ψ a term like $f(t, \vec{x})(|\boldsymbol{F}\vec{a}| - 1)$ one can model the active behavior of a material and then the system can be coupled with additional models of chemical and electric activation of the active response of the tissue, see [22]. In the same manner the constitutive relation for the fluid can be directly extended to the power law models used to describe the shear thinning property of the blood. Further extension to viscoelastic models and coupling with the mixture based model for soft tissues together with models for chemical and electric processes involved in biomechanical problems would allow to perform realistic simulation for real applications.

In order to obtain the solution of a complicated models encountered in biomechanics one has to solve the discrete system resulting from the finite element discretization of the governing equations. This requires sophisticated solvers of

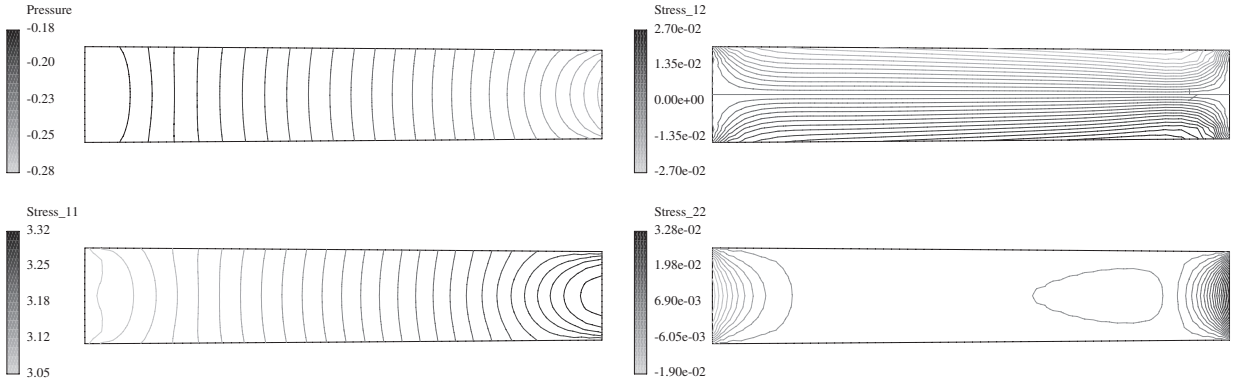

Fig. 23. Isolines of the pressure field and the stress components σ_{12}, σ_{11} and σ_{22}.

nonlinear systems and fast solvers for very large linear systems. The computational complexity increases tremendously for full 3D problems and with more complicated models like visco-elastic materials for the fluid or solid components. The presented numerical method is based on accurate higher order stable finite element discretization and implicit treatment of the interaction. The main advantage of such combination is the overall robustness of the method with respect to the constitutive models by which we mean the fact that a wide range of fluid-structure interaction models from the biomechanics area can be solved by the described algorithm.

The possible directions of improving the efficiency of the solvers include development of fast linear solver based on multigrid ideas, spatial and temporal adaptivity and effective use of parallel computations.

References

[1] E.S. Almeida, R.L. Spilker, Finite element formulations for hyperelastic transversely isotropic biphasic soft tissues, Comput. Meth. Appl. Mech. Eng. 151 (1998) 513–538.
[2] S. Balay, K. Buschelman, W.D. Gropp, D. Kaushik, G.M. Knepley, L.C. McInnes, F.B. Smith, H. Zhang, PETSc: Portable Extensible toolkit for Scientific computation ⟨http://www.mcs.anl.gov/pets⟩.
[3] R. Barrett, M. Berry, T.F. Chan, J. Demmel, J. Donato, J. Dongarra, V. Eijkhout, R. Pozo, C. Romine, H. Van der Vorst, Templates for the Solution of Linear Systems: Building Blocks for Iterative Methods, second ed., SIAM, Philadelphia, PA, 1994.
[4] R. Bramley, X. Wang, SPLIB: A Library of Iterative Methods for Sparse Linear Systems, Department of Computer Science, Indiana University, Bloomington, IN, 1997 ⟨http://www.cs.indiana.edu/ftp/bramley/splib.tar.gz⟩.
[5] K.D. Costa, P.J. Hunter, J.M. Rogers, J.M. Guccione, L.K. Waldman, A.D. McCulloch, A three-dimensional finite element method for large elastic deformations of ventricular myocardum: I—Cylindrical and spherical polar coordinates, Trans. ASME J. Biomech. Eng. 118 (4) (1996) 452–463.
[6] K.D. Costa, P.J. Hunter, J.S. Wayne, L.K. Waldman, J.M. Guccione, A.D. McCulloch, A three-dimensional finite element method for large elastic deformations of ventricular myocardum: II—Prolate spheroidal coordinates, Trans. ASME J. Biomech. Eng. 118 (4) (1996) 464–472.
[7] F. Dai, K.R. Rajagopal, Diffusion of fluids through transversely isotropic solids, Acta Mech. 82 (1990) 61–98.
[8] P.S. Donzelli, R.L. Spilker, P.L. Baehmann, Q. Niu, M.S. Shephard, Automated adaptive analysis of the biphasic equations for soft tissue mechanics using a posteriori error indicators, Int. J. Numer. Methods Eng. 34 (3) (1992) 1015–1033.
[9] C. Farhat, M. Lesoinne, N. Maman, Mixed explicit/implicit time integration of coupled aeroelastic problems: three-field formulation, geometric conservation and distributed solution, Int. J. Numer. Methods Fluids 21 (10) (1995) 807–835 Finite Element Methods in Large-scale Computational Fluid Dynamics, Tokyo, 1994.
[10] Y.C. Fung, Biomechanics: Mechanical Properties of Living Tissues, second ed., Springer, New York, NY, 1993.
[11] S. Geller, M. Krafczyk, J. Tölke, S. Turek, J. Hron, Benchmark computations based on lattice-Boltzmann, finite element and finite volume methods for laminar flows, Comput. & Fluids 35 (2006) 888–897.
[12] M.E. Gurtin, Topics in Finite Elasticity, SIAM, Philadelphia, PA, 1981.
[13] M. Heil, Stokes flow in collapsible tubes: computation and experiment, J. Fluid Mech. 353 (1997) 285–312.
[14] M. Heil, Stokes flow in an elastic tube—a large-displacement fluid-structure interaction problem, Int. J. Numer. Methods Fluids 28 (2) (1998) 243–265.
[15] J. Hron, J.D. Humphrey, K.R. Rajagopal, Material identification of nonlinear solids infused with a fluid, Math. Mech. Solids 7 (6) (2002) 629–646.
[16] J.D. Humphrey, R.K. Strumpf, F.C.P. Yin, Determination of a constitutive relation for passive myocardium: I. A new functional form, J. Biomech. Eng. 112 (3) (1990) 333–339.

[17] J.D. Humphrey, R.K. Strumpf, F.C.P. Yin, Determination of a constitutive relation for passive myocardium: II. Parameter estimation, J. Biomech. Eng. 112 (3) (1990) 340–346.
[18] B. Koobus, C. Farhat, Second-order time-accurate and geometrically conservative implicit schemes for flow computations on unstructured dynamic meshes, Comput. Methods Appl. Mech. Eng. 170 (1–2) (1999) 103–129.
[19] M.K. Kwan, M.W. Lai, V.C. Mow, A finite deformation theory for cartilage and other soft hydrated connective tissues—I, Equilibrium results, J. Biomech. 23 (2) (1990) 145–155.
[20] P. Le Tallec, S. Mani, Numerical analysis of a linearised fluid-structure interaction problem, Numer. Math. 87 (2) (2000) 317–354.
[21] M.E. Levenston, E.H. Frank, A.J. Grodzinsky, Variationally derived 3-field finite element formulations for quasistatic poroelastic analysis of hydrated biological tissues, Comput. Meth. Appl. Mech. Eng. 156 (1998) 231–246.
[22] W. Maurel, Y. Wu, N.M. Thalmann, D. Thalmann, Biomechanical models for soft tissue simulation, ESPRIT Basic Research Series, Springer, Berlin, 1998.
[23] M.I. Miga, K.D. Paulsen, F.E. Kennedy, P.J. Hoopes, D.W. Hartov, A. Roberts, Modeling surgical loads to account for subsurface tissue deformation during stereotactic neurosurgery, in: IEEE SPIE Proceedings of Laser-Tissue Interaction IX, Part B: Soft-tissue Modeling, vol. 3254, 1998, pp. 501–511.
[24] C.W.J. Oomens, D.H. van Campen, A mixture approach to the mechanics of skin, J. Biomech. 20 (9) (1987) 877–885.
[25] K.D. Paulsen, M.I. Miga, F.E. Kennedy, P.J. Hoopes, A. Hartov, D.W. Roberts, A computational model for tracking subsurface tissue deformation during stereotactic neurosurgery, IEEE Trans. Biomed. Eng. 46 (2) (1999) 213–225.
[26] J.M.T. Penrose, C.J. Staples, Implicit fluid-structure coupling for simulation of cardiovascular problems, Int. J. Numer. Methods Fluids 40 (2002) 467–478.
[27] C.S. Peskin, Numerical analysis of blood flow in the heart, J. Computat. Phys. 25 (3) (1977) 220–252.
[28] C.S. Peskin, The fluid dynamics of heart valves: experimental, theoretical, and computational methods, in: Annual Review of Fluid Mechanics, vol. 14, Annual Reviews, Palo Alto, CA, 1982, pp. 235–259.
[29] C.S. Peskin, D.M. McQueen, Modeling prosthetic heart valves for numerical analysis of blood flow in the heart, J. Comput. Phys. 37 (1) (1980) 113–132.
[30] C.S. Peskin, D.M. McQueen, A three-dimensional computational method for blood flow in the heart. I. Immersed elastic fibers in a viscous incompressible fluid, J. Comput. Phys. 81 (2) (1989) 372–405.
[31] A. Quarteroni, Modeling the cardiovascular system: a mathematical challenge, in: B. Engquist, W. Schmid (Eds.), Mathematics Unlimited—2001 and Beyond, Springer, Berlin, 2001, pp. 961–972.
[32] A. Quarteroni, M. Tuveri, A. Veneziani, Computational vascular fluid dynamics: problems, models and methods, Comput. Visual. Sci. 2 (4) (2000) 163–197.
[33] K.R. Rajagopal, L. Tao, Mechanics of Mixtures, World Scientific Publishing Co. Inc., River Edge, NJ, 1995.
[34] R.A. Reynolds, J.D. Humphrey, Steady diffusion within a finitely extended mixture slab, Math. Mech. Solids 3 (2) (1998) 127–147.
[35] M. Rumpf, On equilibria in the interaction of fluids and elastic solids, in: Theory of the Navier–Stokes Equations, World Scientific Publishing, River Edge, NJ, 1998, pp. 136–158.
[36] P.A. Sackinger, P.R. Schunk, R.R. Rao, A Newton–Raphson pseudo-solid domain mapping technique for free and moving boundary problems: a finite element implementation, J. Comput. Phys. 125 (1) (1996) 83–103.
[37] J.J. Shi, Application of theory of a Newtonian fluid and an isotropic non-linear elastic solid to diffusion problems, Ph.D. Thesis, University of Michigan, Ann Arbor, 1973.
[38] R.L. Spilker, J.K. Suh, Formulation and evaluation of a finite element model for the biphasic model of hydrated soft tissues, Comput. Struct., Front. Comput. Mech. 35 (4) (1990) 425–439.
[39] R.L. Spilker, J.K. Suh, V.C. Mow, Finite element formulation of the nonlinear biphasic model for articular cartilage and hydrated soft tissues including strain-dependent permeability, Comput. Meth. Bioeng. 9 (1988) 81–92.
[40] J.K. Suh, R.L. Spilker, M.H. Holmes, Penalty finite element analysis for non-linear mechanics of biphasic hydrated soft tissue under large deformation, Int. J. Numer. Methods Eng. 32 (7) (1991) 1411–1439.
[41] C. Truesdell, A First Course in Rational Continuum Mechanics, vol. 1, second ed., Academic Press, Boston, MA, 1991.
[42] W.J. Vankan, J.M. Huyghe, J.D. Janssen, A. Huson, Poroelasticity of saturated solids with an application to blood perfusion, Int. J. Eng. Sci. 34 (9) (1996) 1019–1031.
[43] W.J. Vankan, J.M. Huyghe, J.D. Janssen, A. Huson, Finite element analysis of blood flow through biological tissue, Int. J. Eng. Sci. 35 (4) (1997) 375–385.
[44] M.E. Vermilyea, R.L. Spilker, Hybrid and mixed-penalty finite elements for 3-d analysis of soft hydrated tissue, Int. J. Numer. Meth. Eng. 36 (24) (1993) 4223–4243.
[45] C. Zoppou, S.I. Barry, G.N. Mercer, Dynamics of human milk extraction: a comparative study of breast-feeding and breast pumping, Bull. Math. Biol. 59 (5) (1997) 953–973.